COO-2597-5

METHODS FOR REDUCING HEAT LOSSES FROM FLAT PLATE SOLAR COLLECTORS. PHASE III

Final Report, May 1, 1977—January 31, 1979

By
K. G. T. Hollands
G. D. Raithby
F. B. Russell
R. G. Wilkinson

March 1979

Work Performed Under Contract No. EY-76-G-02-2597

University of Waterloo
Waterloo, Ontario, Canada

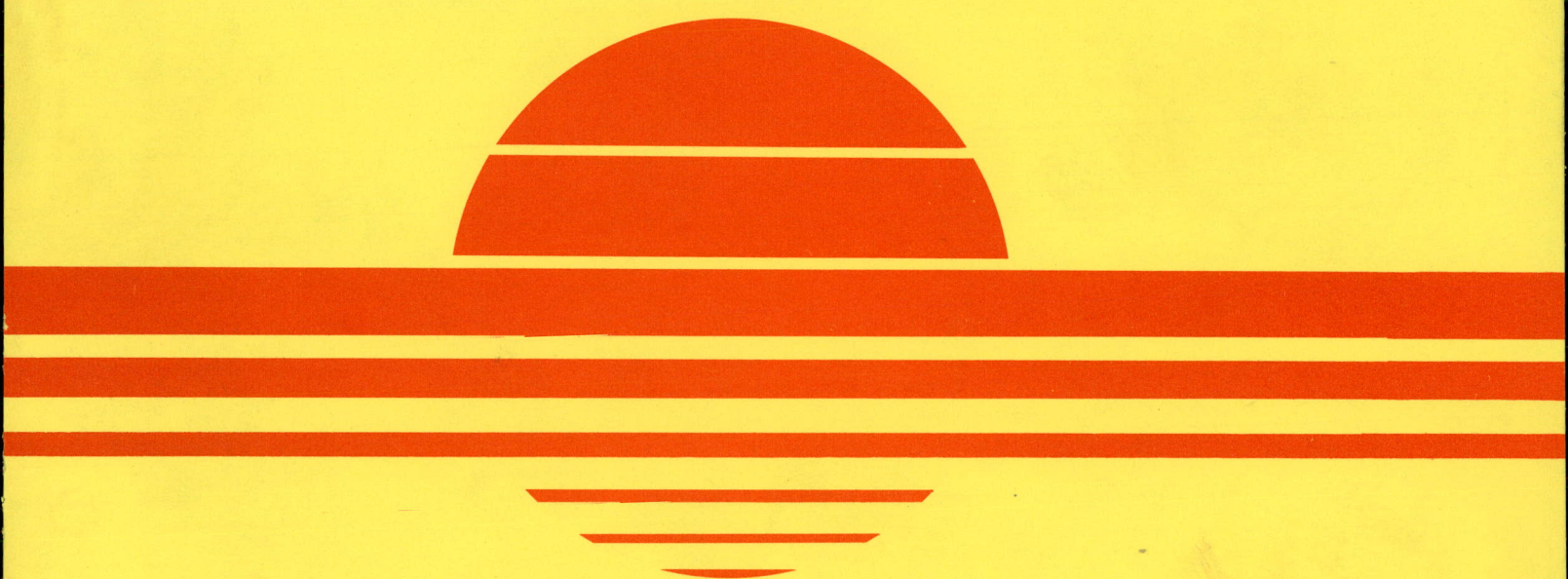

U.S. Department of Energy

Solar Energy

DISCLAIMER

NOTICE

This report has been reproduced directly from the best available copy.

Available from the National Technical Information Service, U. S. Department of Commerce, Springfield, Virginia 22161.

Price: Paper Copy $6.00
Microfiche $3.00

COO-2597-5
Distribution Category UC-59c

METHODS FOR REDUCING HEAT LOSSES FROM FLAT PLATE SOLAR COLLECTORS PHASE III

Final Report

for Period May 1, 1977 to January 31, 1979

WRI Project No. 702-02

K.G.T. Hollands
G.D. Raithby
F.B. Russell
R.G. Wilkinson

University of Waterloo
Waterloo, Ontario, N2L 3G1
Canada

March, 1979

Prepared for

THE U.S. DEPARTMENT OF ENERGY
UNDER GRANT NO. EY-76-G-02-2597.*000 (ERDA)

ABSTRACT

Previous studies in this series have examined heat losses by free convective heat transfer across air layers in flat plate solar collectors, with particular emphasis on the effect of honeycombs on this free convection. The present study extends these earlier studies by examining the effect of the emissivities of both the absorber plate and the glass cover on the honeycomb's ability to suppress free convection, and on the radiative and conductive heat transfer which takes place across the honeycomb in the absence of free convection.

By means of heat transfer measurements on ten Mylar honeycombs, this study has shown that the effect of the above emissivities on the suppression of convection by the honeycomb is slight, and can probably be ignored. On the other hand, the measurements also showed that the effect of these emissivities on the non-convective heat transfer is substantial, but not nearly so large as would have been predicted by existing theories. To explain this latter result theories were developed which take into account the important coupling (ignored by previous theories) between the conductive and radiative modes of heat transfer. These new theories predict the measured heat transfer rates to with about $\pm$ 15%, depending on the emissivities. The results of this study have direct application to evaluating solar collectors which combine a selective surface with a honeycomb.

SUMMARY

This report is mainly devoted to describing work carried out in the third and final phase of the research project entitled "Methods for Reducing Heat Losses from Flat-Plate Solar Collectors", which commenced August 1, 1974. Since it is the last report in the series, it is proper (and contractually required) to include in it a summary of the results of the total project.

Phase One is fully described in a report entitled "Studies on Methods of Reducing Heat Losses from Flat-Plate Solar Collectors",* numbered COO-2597-2 and dated June, 1976. That report described the results of three studies, all of which were related to methods for improving the efficiency of flat plate solar collectors. The first study related to the suppression of free convective heat transfer in an inclined air layer by means of insertion of a honeycomb. It demonstrated experimentally that considerable suppression is possible in the inclined position, a reduction of 80% being observed for a honeycomb of aspect ratio of 5. Equations and charts permitting rational design of honeycombs for convection suppression in solar collectors were given. Details of this study are contained in (1)**.

The second study related to the free convection in an inclined air layer not containing a honeycomb, such as occurs in a conventional flat plate collector. This experimental and theoretical study resulted in a set of relations predicting the free convective heat loss as a function of the relevant variables (2,3). Some recommendations for the best spacing

---

* This report was found to contain typing errors in some of its equations. A list of errata for it is contained in Section 12.

** Numbers in curved brackets denote references contained in Section 11.

between the absorber plate and the transparent cover, and between adjacent transparent covers, were given.

The third study related to the use of a V-corrugated transparent sheet, rather than a flat sheet, as an inner cover in a solar collector. This analytical and experimental study has demonstrated that the solar transmittance of the V-corrugated sheet will generally be higher than the corresponding flat sheet, so that increased collector performance can be expected.

Phase Two is fully described in a report entitled "Methods for Reducing Heat Losses from Flat Plate Solar Collectors - Phase II" numbered COO-2597-4 and dated March, 1978. That report described the results of two studies, both of which were related to methods for improving the efficiency of flat plate solar collectors.

The first dealt with the free convective heat loss from a V-corrugated absorber plate to a plane transparent (glass) cover. Measurements carried out in the University of Waterloo Natural Convection Apparatus gave Nusselt number as a function of Rayleigh number for angles of inclination of the plate from the horizontal ranging from 0 to 60 degrees. The values of the depth ratio (the ratio of the average depth of the air layer to the depth of the V's) investigated were from 1 to 4; the angle of opening of the V's was 60°. Correlation equations were given for the free convective heat transfer (5). It was concluded that the heat transfer is greater than that for two parallel plane plates having the same average spacing, by up to 50% for a depth ratio of unity.

However, for the larger values of the depth ratio, the increase in heat transfer is slight. A method for choosing dimensions so as to minimize heat transfer was described (6).

The second study dealt with the free convective heat transfer occurring in a honeycomb solar collector in which the honeycomb consists simply of a set of horizontal partitions (or slits) oriented normal to the plate. Measurements were carried out using the University of Waterloo Natural Convection Apparatus. Aspect ratios (plate spacing to distance between partitions) of 3, 5 and 10 were investigated, as were slit materials both opaque and transparent to thermal radiation. A significant conclusion was that for angles of inclination of the plate from the horizontal ranging from 70 to 90 degrees, the horizontal slit honeycomb gives superior convection suppression to a square-celled honeycomb, for the same amount of honeycomb wall material. However, for angles less than 45°, horizontal slits are substantially less effective in convection suppression. Correlation equations were presented for the free convective heat transfer for angles of inclination ranging from 0° to 90° (7). Also presented were equations describing the condition for convection suppression by horizontal slits and plots of satisfactor dimensions for a fixed set of conditions (6).

Phase Three is fully described in the present report. It concentrates on the effect, in a honeycomb solar collector, of the emissivities (called the bounding plate emissivities) of the plates bounding the

honeycomb - namely the absorber plate and the glass cover. Studied in this phase were the effect of these emissivities on (i) the convection suppression capability of the honeycomb; and (ii) the heat transfer across the air layer in the absence of free convection. This latter heat transfer which will be achieved in practice if the honeycomb has the proper cell size, is made up of the combined effect of both the radiative and conductive modes of heat transfer.

Heat transfer measurements were carried out on ten hexagonal-celled Mylar honecombs of aspect ratios ranging from 3 to 10. Each honeycomb was tested with three combinations of bounding plate emissivities. The result of these measurements showed that to within $\pm$ 20% the critical Rayleigh number governing the onset of convection was independent of bounding plate emissivities, and was predicted very closely by the method of Sun. On the other hand, the measurements also showed that the dependence of the non-convective heat transfer on the bounding plate emissivities is substantial, but not nearly so great as was predicted by currently available theories. New theories, which accounted for the important radiative-conductive coupling ignored by previous theories, were therefore developed in the present phase. Based upon both numerical and analytical solutions to the governing equations to the problem, they predicted the heat transfer across the honeycomb with an accuracy of $\pm$ 10% (as compared to measurements) if both bounding plate emissivities are high, and to within $\pm$ 20% if one or both of the bounding plate emissivities are low.

Application of the result of these theories to the design of flat plate solar collectors containing both a honeycomb and a selective

surface indicates that unless the honeycomb walls have a very low emissivity, the additional reduction in heat transfer due to the honeycomb is substantially less than what would previously been predicted and may not be sufficient to justify its use in the collector. On the other hand, if the honeycomb walls have an emissivity of .9 or greater, the extra reduction in loss obtained by using a selective surface is very slight, and probably insufficient to justify its use in the collector.

TABLE OF CONTENTS

		Page
ABSTRACT		ii
SUMMARY		iii
TABLE OF CONTENTS		viii
LIST OF FIGURES		x
LIST OF TABLES		xii
1.	INTRODUCTION	1
	1.1 Background	1
	1.2 Definitions and Terminology	3
	1.3 Previous Studies	7
	1.4 Methodology of Present Study	9
2.	DESCRIPTION OF EXPERIMENT AND PRELIMINARY DISCUSSION OF RESULTS	11
	2.1 Experimental Apparatus	11
	2.2 Description of the Honeycombs and Plate Finishes	12
	2.3 Experimental Procedure	14
	2.4 Results	14
3.	DESCRIPTION OF THE THEORY	24
	3.1 Assumptions and Idealizations	24
	3.2 Results of Analysis	
4.	COMPARISON OF EXPERIMENT AND THEORY	35
	4.1 Comparison for Slit Honeycombs	35
	4.2 Comparison for Hexagonal Honeycombs	35
	4.2.1 Numerical Theory	35
	4.2.2 Analytical Theory	42
5.	DISCUSSION OF IMPLICATIONS TO HONEYCOMB COLLECTOR DESIGN	48
6.	CONCLUSIONS	52

TABLE OF CONTENTS (continued):

		Page
7.	LIST OF REFERENCES	53
8.	NOMENCLATURE	55
9.	LIST OF CONTRIBUTING PERSONNEL	59
10.	LIST OF PUBLICATIONS AND PAPERS ISSUED DURING THE TOTAL CONTRACT PERIOD	61
APPENDIX		62

LIST OF FIGURES

		Page
Fig. 1-1	Schematic showing air layer of depth L bounded above and below by isothermal plates at temperatures T_c and T_h respectively. The air layer contains a honeycomb panel of either the "slit"-type (top of Figure) or of the hexagonal-type (bottom of Figure).	4
Fig. 2-1	Measured total heat transfer coefficient h_T for the black-black, black-shiny, and shiny-shiny bounding surfaces respectively. Results for hexagonal-celled honeycombs of two different equivalent diameters are included.	16
Fig. 4-1	Comparison of h_T measurements with predictions from the "Numerical Theory" for diffuse and specular honeycombs, for high emissivity surfaces both below and above a hexagonal celled honeycomb panel.	37
Fig. 4-2	Comparison of h_T measurements with predictions from the "Numerical Theory", for diffuse and specular honeycombs, for a hexagonal-celled honeycomb panel bounded from below by a low emissivity surface and from above by a high emissivity surface.	38
Fig. 4-3	Comparison of h_T measurements with the predictions from the "Numerical Theory", for diffuse and specular honeycombs, for a hexagonal-celled honeycomb panel bounded below and above by low emissivity surfaces.	39
Fig. 4-4	A comparison of measured h_T with values predicted from the "Numerical Theory" in which the honeycomb was assumed to be a diffuse reflector.	40
Fig. 4-5	A comparison of measured h_T with values predicted from the "Numerical Theory" in which the honeycomb was assumed to be a specular reflector.	41
Fig. 4-6	The effect of honeycomb emissivity, ε, on the total heat transfer coefficient for two high emissivity bounding surfaces. The incapability of the diffuse side-wall predictions to reproduce the measured h_T for any value of h_T is of particularly note.	44
Fig. 4-7	A comparison between measured h_T and predictions of the "Analitical Theory" for both specular and diffuse honeycomb assumptions, and for the independent and coupled mode analyses. The top and bottom plates are of high emissivity (BB case).	45

LIST OF FIGURES (cont'd)

		Page
Fig. 4-8	A comparison between measured h_T and predictions of the "Analytical Theory" for both specular and diffuse honeycomb assumptions, and for the independent and coupled mode analyses. The bottom plate has low emissivity and the top plate has high emissivity (SB case).	46
Fig. 4-9	A comparison between measured h_T and predictions of the "Analytical Theory" for both specular and diffuse honeycomb assumptions, and for the independent and coupled mode analyses. Both the bottom and top plates were of low emissivity (S-S case).	47
Fig. 5-1	The dependence of overall heat transfer coefficient on emissivity of the honeycomb material for panels bounded below and above by plates of various emissivities. The predictions are from the "Analytical Theory" using the specular side wall approximation, with a cell aspect ratio of 4.8.	49
Fig. A-1	A single honeycomb cell idealized as a solid cylindrical shell comprised of honeycomb material and a gaseous core.	64
Fig. A-2	A schematic giving nomenclature for the radiant enclosure analysis, detailing the inner of the two cylinders in Fig. A-1.	65

LIST OF TABLES

		Page
Table 2.1	Values of Plate Emissivities for the Three Sets of Tests	13
Table 2.2	Summary of Measured and Predicted Critical Rayleigh Numbers	18
Table 2.3	Total Measured Heat Transfer Coefficients in Stagnant Air Condition, h_T	19
Table 2.4	Independent Mode Predictions of h_T for Diffuse Side Walls	20
Table 2.5	Independent Mode Predictions of h_T for Specular Side Walls	21
Table 3.1	Table of Expressions for the Elements b_{ij} of $\vec{B}$	30
Table 3.2	Table of Expressions for the Elements $\{e_j\}$ of $\vec{E}$	31
Table 3.3	Specular Analysis - Comparison of Analytically Calculated Heat Transfer Coefficients With Numerically Calculated Heat Transfer Coefficients	32
Table 3.4	Diffuse Analysis - Comparison of Analytically Calculated Heat Transfer Coefficients With Numerically Calculated Heat Transfer Coefficients	33
Table 4.1	Comparison of Slit Honeycomb Predictions and Measurement	36

1. INTRODUCTION

1.1 Background

In the first and second phases of the ERDA-supported studies at the University of Waterloo, methods of reducing heat losses from flat plate solar collectors have been examined.[1,2] The studies have concentrated largely on the free convective heat transfer taking place in solar collectors of both honeycomb and non-honeycomb types. Topics examined have included:

i) free convective heat transfer across inclined air layers constrained by honeycombs of cell shapes consisting of squares, hexagons and long rectangles;

ii) free convective heat transfer across inclined air layers not constrained by a honeycomb, having both planar and V-corrugated boundaries.

The honeycomb work has resulted in correlation equations which permit the design of a honeycomb to suppress free convection currents with what is thought to be reasonable accuracy. However, these equations resulted from measurements made on the University of Waterloo Natural Convection Apparatus and in this apparatus, the upper and lower bounding surfaces (corresponding to the glass cover and the absorber plate in the solar collector) are polished copper plates having low emissivity, whereas in actual application, both plates may be expected to have high emissivity (e.g. a standard glass cover and a black-painted absorber plate); or one may have low emissivity and one high (e.g. a standard glass cover and a selective surface absorber plate). Since it is known that the effect of thermal radiation on the free convective heat transfer across

honeycombs is substantial, it was decided to check this work in the third phase, using plate emissivities more closely approximating those actually found in solar collectors.

A second, more important aspect of the present third phase has had to do with the heat transfer across the honeycomb in the situation where convection is suppressed - i.e. the heat transfer by radiation and gaseous conduction. This situation (called the stagnant air condition), ordinarily holds in the collector provided the honeycomb cell size has been properly chosen. It has generally been considered that the honeycomb reduces the radiant heat loss across the air layer as well as suppressing free convection, but it is now realized that this assumption holds only when both bounding surfaces to the honeycomb are of high emissivity (e.g. in a solar collector having a standard glass cover and a black painted absorber plate). As was initially indicated by collector performance measurements at the Lockheed Palo Alto Research Labs [3], and verified by experiments on rectangular honeycombs at the University of Waterloo in phase 2 [2], if one or both of the bounding plate emissivities is low, the effect of the honeycomb is to give an apparent <u>increase</u> in the radiative transfer. Such an increase must therefore be expected if a selective surface and honeycomb are combined in one collector. This combination has otherwise appeared very interesting for plastic honeycombs since (in contrast to glass), most plastics lack the high opacity to long wave radiation required for good radiant suppression in a honeycomb. Hence a plastic honeycomb would have appeared to benefit from a selective surface to give the radiant suppression, the honeycomb then supplying mainly convection suppression. The combination may still be

attractive, since the radiant increase by the honeycomb is not necessarily large. However, it cannot be properly evaluated until a theory is available for predicting the total heat loss.

Starting from the paper of Hollands[4] in 1965, all available theories for calculating heat transfer across honeycombs in the stagnant air condition predict that the honeycomb will always decrease the radiant heat transfer across the air layer. It is now clear therefore that these theories are incorrect and need revising. The basic premise which appears to be in error is the "independent mode" hypothesis. This hypothesis, which states that the two relevant modes of heat transfer, namely conduction (through the air and the walls) and thermal radiation, act completely independently of each other so that one can calculate the first, ignoring the presence of the second, and vice-versa, the total heat transfer then being the sum of the two.

For reasons which will be discussed later, this assumption, although reasonable for the case where both bounding plates to the honeycomb have high emissivity, breaks down when one or both have a low emissivity. A major objective of the present phase 3 was to develop a theory which would make this heat transfer predictable with reasonable confidence. Once this is done, the viability of the combination of a plastic honeycomb and a selective surface can be established.

1.2 Definitions and Terminology

The two types of honeycombs considered in this report are shown in Figure 1.1. The set of horizontal slits shown in the upper sketch can be fabricated from plastic film, wound tightly on a frame. The second, the traditional hexagonal type of engineering honeycomb, is the honeycomb

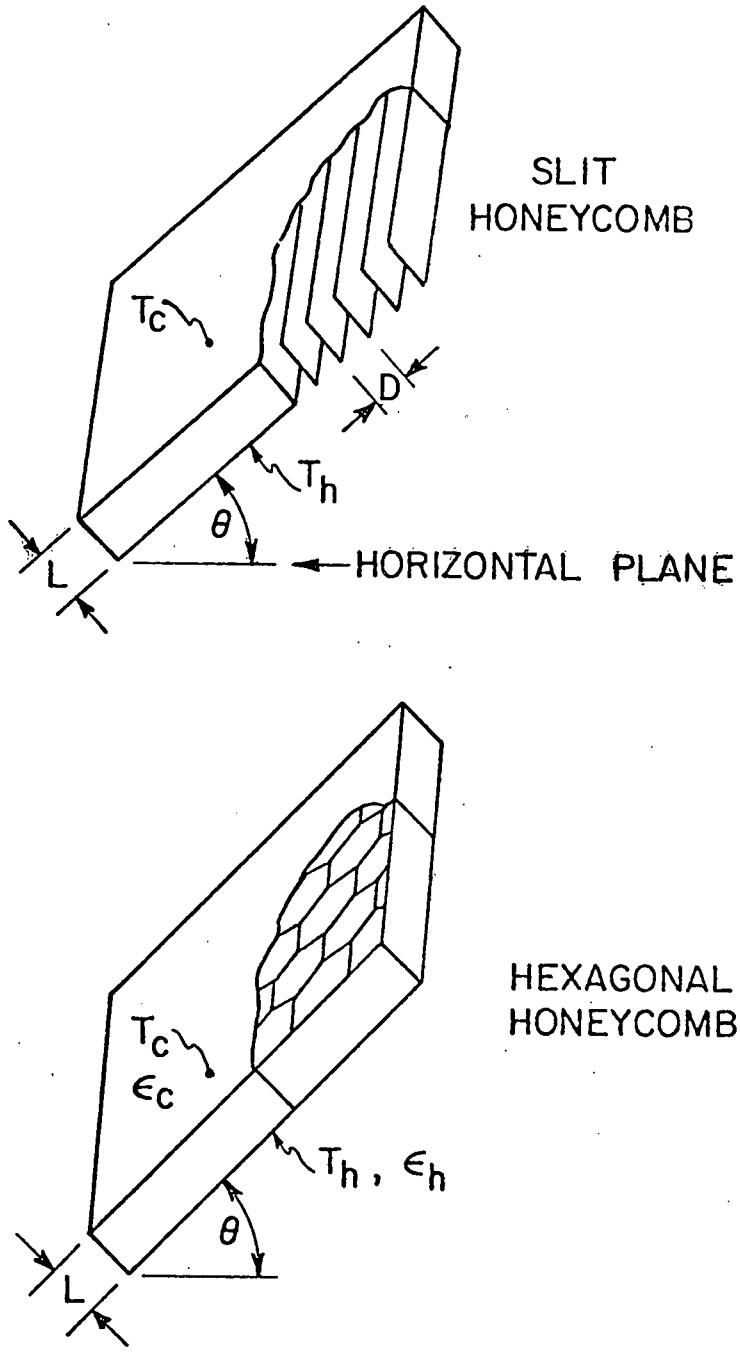

Fig. 1-1 Schematic showing air layer of depth L bounded above and below by isothermal plates at temperatures T_c and T_h respectively. The air layer contains a honeycomb panel of either the "slit"-type (top of Figure) or of the hexagonal-type (bottom of Figure).

which was used in the present experimental program. In either case the honeycomb consists essentially of partitions running from the hot plate to the cold plate; these partitions will be called side-walls. The plates bounding the honeycomb on each face form the end-walls to an individual cell and are therefore called end-walls.

The honeycomb cells can be characterized by the aspect ratio A defined by:

$$A = L/D$$

The distance L is the spacing between the two bounding plates. For the slit, D is the spacing between the adjacent slits. For the hexagonal cell, D is the diameter of a circle which has the same area as a cross section of the hexagonal cell.

The emissivity of the side-walls are denoted by ϵ, and ϵ_c and ϵ_h are the emissivities of the plates bounding the honeycomb on the cold and hot face respectively, - i.e. of the end-walls.

The term stagnant air will be used to indicate that the air layer in the honeycomb is motionless, the free convective motion being suppressed. The honeycomb inserted into a horizontal air layer suppresses convective currents for all Rayleigh numbers, Ra, less than a critical value, denoted by Ra_c, the Rayleigh number being defined by:

$$Ra = g\,\beta(T_h - T_c)\,L^3/(\nu\lambda) \qquad 1\text{-}1$$

By assuming the air obeys the ideal gas law, it is possible to express Ra in terms of the fluid pressure:

$$Ra = \frac{P^2(T_h - T_c)\,g\,L^3}{\mu^2\,\bar{R}^2\,T^2}\,.\,Pr \qquad 1\text{-}2$$

Hence, in the experiments, for a given plate spacing and temperature difference, the Rayleigh number could be varied by changing the fluid pressure.

The overall heat transfer coefficient, from the lower to the upper plate is denoted by h_T in the stagnant air situation, and if convection is occurring, it is denoted by $h_{T,c}$. It is convenient to define h_c as the conduction heat transfer coefficient which would exist if their were no coupling between the radiant and conductive modes. It is given by:

$$h_c = k_e/L \qquad 1\text{-}3$$

where k_e is the effective thermal conductivity, combining the effects of the thermal conductivity of air k_a and of side-wall, k_w:

$$k_e = \frac{k_g A_{c,g} + k_s A_{c,s}}{A_{c,g} + A_{c,s}} \qquad 1\text{-}4$$

$A_{c,g}$ and $A_{c,s}$ are the areas of air and side-wall which are exposed on a cross-section of a single honeycomb cell.

The quantity h_r will be defined by:

$$h_r = h_T - h_c$$

If the two modes are completely decoupled, h_r represents the radiant component of the total heat transfer.

The Nusselt number - the dimensionless free convective heat transfer across the honeycomb - is defined by:

$$Nu = 1 + (h_{T,c} - h_T)\, L/k_g \qquad 1\text{-}5$$

where it is recalled that subscript c on h_T denotes the convecting situation.

1.3 Previous Studies

Early work on radiant heat transfer in passages such as exist in individual honeycomb cells, was performed by Hottel and Keller (1933) [6], who were concerned with radiant loss through openings in furnace walls. They treated a cavity with black isothermal end walls at different temperatures T_h and T_c and assumed the side walls of the cavity were adiabatic and diffusely emitting and reflecting. The gas in the cavity was assumed to be non-conducting. They presented their results in terms of a radiant "interchange factor", $\overline{F}$ defined by

$$\overline{F} = q_r/\sigma(T_h^4 - T_c^4) \qquad 1\text{-}6$$

where q_r is the radiant flux across the cavity. Hollands, [4], extended this result by noting that, if the end walls are not black but have emissivities ϵ_h and ϵ_c, the flux is given by:

$$q_r = \overline{F}' \sigma(T_h^4 - T_c^4) \qquad 1\text{-}7$$

where:

$$\frac{1}{\overline{F}'} = \frac{1}{\overline{F}} + \frac{(1 - \epsilon_c)}{\epsilon_c} + \frac{(1 - \epsilon_h)}{\epsilon_h} \qquad 1\text{-}8$$

and $\overline{F}$ is the same as that given by Hottel and Keller. This result is strictly valid only for uniform heat flux boundary conditions on the end walls rather than uniform temperature boundary conditions but the dependence on this boundary condition is expected to be slight in high aspect ratio cells. Edwards and Tobin [7] extended Hottel and Kellers result to specularly reflecting side-walls, allowing also for the effect of polarization on the reflectivity of the side-walls. Perlmutter and Siegel [9] reported an expression for the specular form factor between elemental

areas in a cylindrical cavity and discuss its approximate representation by an exponential function. Tien and Yuen [8] applied the results of Edwards and Tobin specifically to honeycombs in honeycomb solar collectors. They were able to demonstrate a close analogy between this problem and that of radiant exchange across an absorbing-emitting non-conducting gas between parallel plates and in this way they were able to obtain a closed form expression for the radiant exchange factor across a honeycomb. They compared their predictions with measured heat transfer across honeycombs carried out in high vacuum (so high that the gaseous thermal conductivity was eliminated) and found good agreement. Buchberg and Edwards [10] and Felland and Edwards[11] have recently reported detailed calculations and measurements of heat transfer across glass honeycombs.

All of the preceding papers either ignored the effect of conduction in the side wall and in the gas, or they made the 'independent mode' assumption. According to this assumption, as outlined by Hollands [4], each mode of heat transfer is calculated independently of the other. Thus the conduction heat transfer coefficient, h_c, is calculated from 1-3 and 1-4 and the radiant heat transfer coefficient, h_r, is calculated from:

$$h_r = q_r/(T_h - T_c) = \bar{F}' \sigma(T_h^4 - T_c^4)/(T_h - T_c) \qquad 1\text{-}9$$

the total heat transfer coefficient being given simply from:

$$h_T = h_c + h_r \qquad 1\text{-}10$$

The quantity $\bar{F}'$ is given by equation 1-8 for diffusely reflecting side-walls and by a similar expression, such as may be obtained from Tien and Yuen's study, for specular reflecting side-walls.

1.4 Methodology of Present Study

The method of the present study can be divided into an experimental part and a theoretical part. The experimental part consisted of measurements on ten hexagonal-celled Mylar honeycombs which had been developed for use in solar collectors. These measurements included the critical Rayleigh number, Ra_c, and the total heat transfer coefficient across the honeycomb in the stagnant air condition, h_T. They were carried out for each honeycomb and for each of three combinations of the emissivities of the plates bounding the honeycomb. The theoretical part consisted of writing down and solving the equations governing coupled radiative and conductive heat transfer in a honeycomb cell, and from these solutions, calculating h_T. In order to obtain solutions, various approximations had to be made. Two approaches were taken. The first was to solve the integro-differential governing equation numerically. This approach generally made the fewest assumptions but closed form analytical expressions for the heat transfer were not obtained. The second which solved the governing equations analytically, yielded analytical expressions for the heat transfer. In order to obtain a solution in this case, several approximations had to be made. Consequently this approach was more approximate than the numerical approach.

In addition to the measurements on heat transfer across hexagonal honeycombs outlined above, another set of measurements on horizontal slit type honeycombs were available for comparison with the various theories. These measurements were carried out by Smart [5] and reported in the phase

2 report [2].

Comparison of the results of the two theoretical approaches with each other and with the two sets of experimental results has permitted conclusions to be made on the validity of the theories. From the results, the viability of the combination of plastic honeycombs and selective surface has been examined.

2. DESCRIPTION OF EXPERIMENT AND PRELIMINARY DISCUSSION OF RESULTS

2.1 Experimental Apparatus

The series of experiments reported in this study were carried out on the University of Waterloo Natural Convection Appartus which has been fully described previously [12,13]. Only recent modifications and basic measurement techniques are described.

The air layer is contained in a pressure vessel with an air supply allowing a pressure variation of from 1 to 700 k Pa. In this way changing the Rayleigh number can be accomplished by changing the pressure. A set of parallel copper plates were placed horizontally inside the vessel with the honeycomb between them. The plates measured 56 cm x 61 cm, and their spacing could be adjusted up to 12.7 cm. A temperature difference was maintained between them by means of water circulated through copper tubes soldered on their back faces, the water temperatures being maintained constant by two constant temperature baths.

Measurements of the total heat flux were made in a 5" x 5" (12.7 cm x 12.7 cm) area, in the middle of the lower plate. Recessed into the plate were an electrical heater plate and a heat flux meter. The heater plate was heated electrically until the plate was almost isothermal with the lower plate. Heat transfer readings were made by converting the heater current into a heat flux, and accounting for the small heat flow through the heat flux meter. Due to the occassional unsteady nature of the heat flux, the heat flux meter emf was averaged by sampling 600 times over 40 minutes, for most data points. The mean and standard deviation were recorded, and a strip chart recording made. A nominal temperature difference of 7.8 C was maintained, at a mean temperature of 28.9 C.

2.2 Description of the Honeycombs and Plate Finishes

The stagnant air heat transfer coefficient, h_T, across honeycombs, was measured for 10 different hexagonal honeycombs made of Mylar- a Dupont trade name for a polyester plastic. The honeycombs were fabricated commercially by Hexcel Co. of Dublin, California, under the trade name Solar-core. The bounding copper plates were, in the first instance, both painted black to obtain an emissivity of .88. These tests with both plates painted black were designated by BB. The second set of tests (denoted by SB) had the lower plate changed to a polished copper state with an emissivity of .065. The third set had both plates polished copper and was denoted SS. Table 2-1 summarizes the emissivities for each of the combinations.

Two cell sizes of honeycombs were tested. Seven honeycombs of nominal cell size 0.95 cm (numbered H1 to H7), and three with 1.27 cm cells numbered H8 to H10 were used. The values of A for these honeycombs ranged from 2.67 to 10.67 (see Table 2-2). Different lengths, L, allowed for variation of the cell aspect ratio. The average wall thickness was measured to be .1 mm. The whole honeycomb structure covered the majority of the area of the plate. With the honeycomb positioned centrally on the bottom plate, the upper plate was lowered onto the honeycomb; although there was contact between parts of the upper plate and honeycomb, a flush fit could not be guaranteed due to the variations in the length of the honeycomb. The plate spacing was measured at 8 locations and averaged. The radiant properties of the Mylar film, for a black body source at room temperature, were measured on a Gier-Dunkle Infrared Reflectometer (model DB 100), with the following results:

TABLE 2-1

Values of Plate Emissivities for the Three Sets of Tests

Test Designation	ϵ_h	ϵ_c
BB	.88	.88
SB	.065	.88
SS	.065	.065

reflectivity ρ = .113 transmissivity τ = .452 and absorptivity α = .435. Provided the honeycomb is at or near room temperature, as it was during the test, then Kirchhoff's law applies, and $\epsilon = \alpha$ = .435.

2.3 Experimental Procedure

For each data point taken, the heater plate current, heat flux meter emf, plate temperature difference (using thermocouples imbedded in the plates), and the air pressure were recorded. All data reduction was carried out using the correlations for property values used by Ruth [14].

The stagnant air total heat transfer coefficient h_T, was measured with the pressure sufficiently low to ensure stagnant air. Further increases in pressure produced no significant variations in heat transfer until a critical pressure was reached after which the heat increased strongly with pressure. The Rayleigh number corresponding to the critical pressure (see equation 1-2) is the critical Rayleigh number. In this way the critical Rayleigh number was determined for each honeycomb.

The data recording system of the Natural Convection Apparatus was modified so as to allow automatic control of some measurement functions using a programmable calculator. Throughout one test, the pressure was set, time was allowed for stabilization, and then all measurements taken, averaged and recorded, all without the need for an operator to be present. This freed the experimenters from many repetitive tasks.

2.4 Results

All raw and reduced data are found in Reference [17]. This includes all 10 honeycombs for the BB tests, and 9 for the SB and SS series. All other relevent test information also available in [17], including plate spacing, operating temperatures and test aspect ratios.

The critical Rayleigh number data are summarized in Table 2.2. Also shown are the calculated values of Ra_c based on the approximate theory of Sun which does not incorporate the effect of ϵ_h and ϵ_c. Attention should be concentrated on the first seven honeycombs since they exhibited much greater uniformity in cell size. At low aspect ratio, statistically there is no significant difference between the three measured Ra_c's. However, as A is increased the SB combination gives Ra_c's which are significantly lower than those for SS and BB. The average deviation of the measured and theoretical Ra_c's is 4.7% in the BB case, 7.7% in the SS case and 20.3% in the SB case. The average value of (Ra_c theory)/(Ra_c measured) was 1.03 for the BB case, 1.018 for the SS case and 1.22 for the SB case. The former two values are not, at a 95% confidence level, significantly different from unity. The last value, corresponding to the SB case was considered statistically different from unity. In summary it may be stated that for hexagonal honeycombs the effect of ϵ_c and ϵ_h on Ra_c is weak, particularly at low aspect ratio and/or provided $\epsilon_h \approx \epsilon_c$. For the purposes of solar engineering calculations it can probably be ignored. Predictions of Ra_c should be based on the method of Sun. No further reference will be made to the Ra_c result. The rest of the report will concentrate on the measurement and predictability of h_T.

The heat transfer data are summarized in Table 2-3 and plotted in Figure 2-1. It is noted that for a given set of plate emissivities, the heat transfer decreased for increased aspect ratio. This decrease was expected, since the independent mode analysis predicted

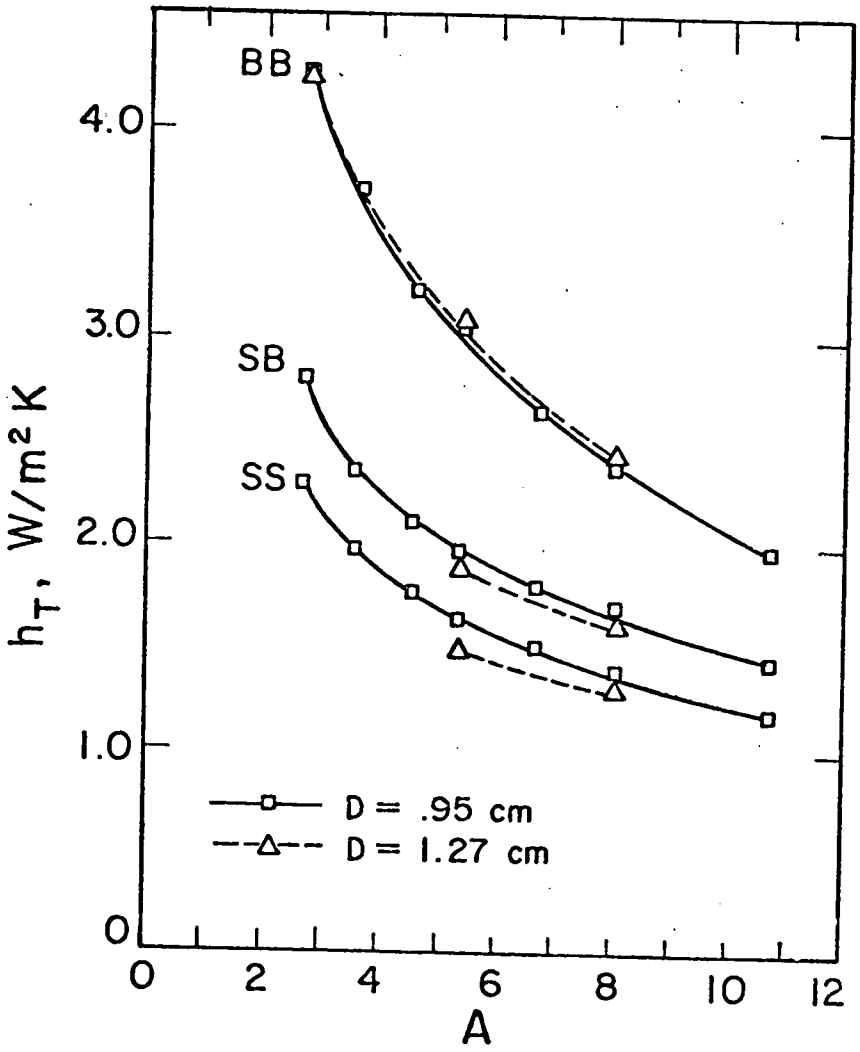

Fig. 2-1 Measured total heat transfer coefficient h_T for the black-black, black-shiny, and shiny-shiny bounding surfaces respectively. Results for hexagonal-celled honeycombs of two different equivalent diameters are included.

that both the conduction and radiation to decrease with length, L, for a fixed D.

For a given honeycomb, the heat transfer was a maximum for the BB test, less for SB and a minimum for the SS test. This is also consistant with the independent mode analysis, since the equivalent form factor, or script factor $\overline{F}'$ for the radiant exchange, based on Hollands [4], is a maximum for black plates, and lowest for low emissivity plates.

2.5 Comparison of Results to the Independent Mode Analysis

As noted above, the h_T data were in qualitative agreement with the independent mode theory. Attention is now focussed on a quantitative comparison. The side wall is first considered to emit and reflect in a diffuse manner. To apply the independent mode model, the total radiation factor, $\overline{F}$, is required from Hottel and Keller [6], who did not unfortunately present data for a hexagonal shape; the hexagon was therefore modelled as a circular cylinder of equal cross sectional area.+ The predictions of h_T by this model for the experimental conditions are presented in Table 2.4 which also shows the % differences of the predicted h_T's from the measured values. The error was found to be in the range -34% to -66%. Thus this analysis, although straight forward, is not accurate.

One source of error may be that the side wall reflects specularly. To apply the analysis for this assumption, the total radiation factor must be obtained. Tien and Yuen [15] presented a method for doing so, but the use of their results was not straight forward since it required the passage transmittance for the specific honeycombs under test. In Appendix A an analysis similar to that of Tien and Yuen, (in that both use the exponential kernel substitution technique), has yielded a closed form expression for

+Data for different shapes was found to correlate closely by using this method.

TABLE 2-2

SUMMARY OF MEASURED AND PREDICTED

CRITICAL RAYLEIGH NUMBERS

		Measured Ra_c's ($X10^{-5}$)			Ra_c calculated $X10^{-5}$ from Sun [16]
Plate emissivity code →		BB	SB	SS	
Honeycomb No.	Aspect ratio				
H1	2.67	.872	.983	.911	.960
H2	3.55	2.51	2.63	2.76	2.64
H3	4.50	6.83	6.07	7.02	6.63
H4	5.33	12.8	12.0	14.0	12.9
H5	6.67	29.5	23.3	31.1	31.4
H6	8.00	62.4	45.5	59.3	63.5
H7	10.67	197.	127.	168.	197
H8	2.67	.717	+	+	.984
H9	5.34	8.35	8.06	10.0	13.3
H10	8.00	45.1	++	62.1	65.5

\+ no measurement made in this case

++ measurement considered unsatisfactory due to lack of cell integrity of the honeycomb

TABLE 2-3

TOTAL MEASURED HEAT TRANSFER COEFFICIENTS

IN STAGNANT AIR CONDITION, h_T

Honeycomb number	Aspect ratio	h_T (W/m^2K)		
		BB+	SB+	SS+
H01	2.67	4.27	2.78	2.26
H02	3.55	3.70	2.33	1.95
H03	4.53	3.21	2.09	1.74
H04	5.33	3.04	1.95	1.61
H05	6.67	2.63	1.79	1.49
H06	8.00	2.36	1.66	1.37
H07	10.67	1.96	1.43	1.17
H08	2.67	4.25	---	---
H09	5.34	3.05	1.86	1.46
H10	8.00	2.41	1.60	1.27

+See Table 2-1 for meaning of BB, SB and SS

TABLE 2-4

INDEPENDENT MODE PREDICTIONS OF h_T FOR DIFFUSE SIDE WALL

Honeycomb number	h_T,BB	% error	h_T,SB	% error	h_T,SS	% error
	(W/m^2K)		W/m^2K		W/m^2K	
H1	2.80	-34	1.39	-50	1.23	-45
H2	2.21	-40	1.12	-52	.977	-50
H3	1.81	-44	.937	-55	.801	-54
H4	1.60	-47	.835	-57	.704	-56
H5	1.32	-50	.710	-60	.591	-60
H6	1.14	-52	.630	-62	.518	-62
H7	.874	-55	.516	-64	.421	-64
H8	2.54	-40	1.13	---	.971	---
H9	1.47	-52	.647	-65	.573	-61
H10	1.05	-56	.542	-66	.432	-66
Average error - %		-47		-59		-58

TABLE 2-5

INDEPENDENT MODE PREDICTIONS OF h_T FOR SPECULAR SIDE WALLS

Honeycomb number	$h_{T,BB}$	% error	$h_{T,SB}$	% error	$h_{T,SS}$	% error
	(W/m^2K)		W/m^2K		W/m^2K	
H1	3.68	-14	1.41	-49	1.24	-45
H2	3.05	-17	1.15	-51	.982	-50
H3	2.58	-19	.970	-54	.812	-53
H4	2.29	-25	.875	-55	.715	-56
H5	1.93	-26	.755	-58	.608	-60
H6	1.68	-29	.675	-59	.536	-61
H7	1.33	-32	.573	-60	.443	-62
H8	3.42	-20	1.15	---	.925	---
H9	2.16	-29	.745	-60	.585	-60
H10	1.37	-43	.590	-63	.450	-65
Average error - %		25%		56%		57%

for the total radiation factor F for a specularly reflecting side wall of a circular cylinder namely:

$$\overline{F} = 1/(1 + \epsilon A)$$

The predictions of this model for the experimental conditions are summarized in Table 2-5. The agreement in the BB results has improved, with the average error being roughly halved to 25%. However, the predictions for the SB and SS series were not improved significantly. The average error still being about 57%. Thus, for both the diffuse and specular independent mode theory, the predictions are consistently low.

The fact that interaction between the two modes must be occuring can best be understood by examining the temperature profiles in the wall which each mode would take up in the absence of the other. Pure conduction would establish a linear profile on the wall with the wall being at T_h on its lower end and T_c at its upper end. Pure radiation would establish a situation whereby, (to a reasonable approximation, see Appendix A) the fourth power of the wall temperature is linear in distance; more importantly, a temperature jump would be established at the plates so that the wall temperature is not equal to T_h at its lower end and T_c at its upper end. The magnitude of this temperature jump is small for black plates and large for low emissivity plates. It is seen that in the case where both radiation and conduction are present the wall cannot take up a temperature which would satisfy each mode independently and consequently the independent mode analysis must be expected to be in error by an amount which is larger when one or both of the plates has a low emissivity. If conduction is present, local thermodynamic equilibrium prevents any jump in temperature. Consequently, in order to eliminate the jump excess heat must be conducted

into the wall at the bottom end. This heat is radiated up the cell and then conducted out at the top end.

The following sections described theories which attempt to quantify this phenomenan.

3. DESCRIPTION OF THE THEORY

Theories, both numerical and analytical have been developed to describe the coupled heat transfer in the honeycomb cells for both the hexagonal and slit-type honeycombs. This section describes these theories.

3.1 Assumptions and Idealizations

In order to simplify the problem and to make the governing equations amenable to solution, a number of assumptions have been made. These assumptions include two categories: those which were always made (the fixed assumptions) and those which appear as options for the various models (the optional assumptions).

Fixed Assumptions

In all instances the analysis was confined to a single model cell which was then taken as representative of a typical cell of the total honeycomb. The thickness, (denoted by t), of its side-wall was taken as equal to one-half of the width of the side-walls of the honeycomb. Since there was no reason to expect net heat transfer from one honeycomb cell to another, the side boundaries of the model cell were taken as adiabatic. In addition to this the following fixed assumptions also applied:

(1) All surfaces of the cell are assumed gray (i.e. all radiant properties are assumed independent of wavelength over the wavelength range of interest (3 to 30 μm)).

(2) All surfaces are assumed diffuse emitters. The plates bounding the cell at top and bottom are also assumed to be diffuse reflectors.

(3) Although the materials used in the honeycomb walls were in fact partly transparent to thermal radiation, with total transmittance τ, total reflectance ρ and total absorptance α, (equal to its total emissivity, ϵ), the side walls of themodel cell were assumed to be opaque with effective total reflectance $\rho_e = \rho + \tau$ and effective emittance ϵ. As indicated by Cane et al [15], this assumption is permitted because of the symmetry about the centre plane of any honeycomb side-wall

(4) The gas (air) inside the cell is assumed to be transparent to thermal radiation.

(5) The air in the cell is assumed to be stagnant.

(6) The hexagonal cell was assumed to be treatable as a cylindrical cell of same cross-sectional area as the hexagon. Pure radiant analyses revealed this to be a very good approximation.

(7) The lower and upper plates bounding the honeycomb cell at top and bottom were taken to be isothermal.

Optional Assumptions

(1) Diffuse vs specular side-wall reflection. A cell as described above constitutes a radiant enclosure for which standard analytical methods are well developed. These analytical methods require that the side walls be described as either perfectly specularly reflecting or perfectly diffusely reflecting, or some linear mixture of the two. The last of these three possibilities was not considered due to the complexities it introduces. Since a simple inspection of the plastic films from which the honeycombs were fabricated (called hereafter the homeycomb films) could not reveal with confidence whether the specular or the diffuse assumption was better, it was decided to carry out

analyses for both types of reflection, and decide which is more valid on the basis of comparison of the predictions of each with the experimental results. Since the equivalent side-wall reflectivity ρ_e is made up of reflected and transmitted components ($\rho_e = \rho + \tau$) decisions as to whether the cell side-wall should be treated as specular or diffuse must take into account the transmission as well as reflection. If, when radiation is incident on a honeycomb film, the transmitted radiation is transmitted along (or nearly along) the same straight line along which it was incident, then the transmitted portion of ρ_e must be treated as specular reflection. If on the other hand the transmitted radiation is uniformly scattered, then the transmitted portion of ρ_e should be taken as diffuse. Since the films had relatively smooth surfaces and since the scattering of radiation inside the film was expected to be slight, the perfectly specular model was expected to be the better approximation.

For the case of the hexagonal honeycomb, analyses were developed for both diffuse and specular models; for the slit type honeycomb only the diffuse model was analyzed.

(2) The 2D vs 1D temperature field. The temperature field of the air inside the honeycomb, in a rigorous approach, must be treated as fully two-dimensional - i.e. dependent upon both vertical and horizontal co-ordinates, the cell axes being taken as vertical. However, if the aspect ratios are relatively high, as is the case with the present experiments, then due to the slenderness of the cells, the temperature gradients in the horizontal direction may be negligible. The assumption that they are constitutes the 1D assumption. In this 1D model, the side-wall and the air can be treated

as parallel resistances to heat flow. The cell may then be modelled as evacuated and the product of thermal conductivity and cross-sectional area for its side-wall may be taken as equal to a value which is the sum of these products for the air and wall separately.

In neglecting the temperature gradients in the horizontal direction, the interaction between the wall and gas may not be treated fully. This is most likely to be in error close to the end plates. To investigate the difference between the 1D model and the more rigorous 2D approach, the full two-dimensional equations were derived, solved numerically and the solutions compared.

(3) The exponential kernel approximation. In this approximation, exact expressions for the radiant configuration factors governing radiant exchange inside the cell are approximated by an exponential-type expression. This approximation was only made for the circular honeycomb cell but it was implemented for both diffuse and specular cases. The approximation in the diffuse case is:

$$1 - \frac{2z^3 + 3z}{2(z^2 + 1)^{3/2}} \approx e^{-2z} \qquad 3\text{-}1$$

(4) Temperature linearization approximation. Provided the temperature of the lower plate T_h does not differ too much from the temperature of the upper plate T_c, then the fourth power of the temperature of the wall T_w, at any height can be approximation by:

$$T_w^4 \approx T_c^4 + \frac{(T_h^4 - T_c^4)}{(T_h - T_c)} (T_w - T_c) \qquad 3\text{-}2$$

This approximation appears reasonable provided $T_h/T_c < \sim 1.2$ where both T_h and T_c are absolute temperatures.

The last three assumptions permitted fully analytical solutions to the governing equations to be obtained, and explicit expressions for h_T to be derived for either the specular or diffuse assumption. Validity of the various assumptions were checked by comparing with the numerical method of solution, which did not (necessarily) invoke any of the last 3 assumptions. (although it required considerably more computational effort if the 1D assumption was not made) Except for special runs, the numerical approach did not make Optional Assumptions 3 and 4, since they created very little reduction in computer time.

3.2 Results of Analysis

Detailed descriptions of the analytical and numerical theories are given in the Appendix. Presentation of the results of the numerical approach will be given in the next section. The equations resulting from the analytical approach for the hexagonal cell, which are based on the 1D assumption and the exponential kernel and temperature linearization approximations are as follows:

$$h_T = -\frac{k_e}{D}\left[\gamma_2 + P(\gamma_3 - \gamma_4)\right] + \epsilon_h \sigma \left[T_h^4 - \gamma_5(T_h^4 - T_c^4)\right]/((T_h - T_c)(1 - \epsilon_h)) \qquad 3\text{-}3$$

where:

$$P = W + 4\,\epsilon^n \qquad 3\text{-}4$$

$$W = \frac{4\,e\,\sigma\,(T_h^4 - T_c^4)\,D}{k_e(T_h - T_c)} + \frac{1}{(1 + \frac{2t}{D})^2} \qquad 3\text{-}5$$

with n = 1 for the diffuse case and n = 2 for the specular case, and where k_e (from 1 - 5) is (assuming D << t):

$$k_e = \frac{k_g D + 4k_s t}{D + 4t} \qquad 3\text{-}6$$

The quanties γ_2, γ_3, γ_4 and γ_5 are the 2nd, 3rd, 4th and 5th elements of the row vector $\vec{\gamma} = \{ \gamma_1, \gamma_2, \gamma_3, \gamma_4, \gamma_5, \gamma_6 \}$ which satisfies the system of linear simultaneous equations:

$$\vec{B}\ \vec{\gamma}' = \vec{E} \qquad 3\text{-}7$$

where $\vec{\gamma}'$ is $\vec{\gamma}$ transposed to a column and the 36 elements of the matrix $\vec{B}$, namely the set $\{b_{ij}\}$, and the six elements of the column $\vec{E}$, namely the set $\{e_j\}$, are functions of the various cell properties. These functions are given in Tables 3-1 and 3-2.

Tables 3-3 and 3-4 compare the values of h_T predicted by the two methods (analytical and numerical) described above. Table 3-3 is for the diffuse case and 3-4 for the specular case. Both assume 1D conduction. The error involved in the approximations of the analytical method are seen to increase with aspect ratio. For the diffuse case they are generally acceptable. For the specular case, errors of the order of 15-20% can be expected, depending on the aspect ratio.

Comparisons between the 1D and 2D conduction models indicated that for the hexagonal honeycomb (circular cell) of the size and properties tested, the error introduced by the 1D model is very small - always less than 1%. For the slit honeycombs, however, of 1.27 cell size, small but significant errors were introduced by the 1D approximation. For honeycombs of the properties and sizes of the 6 slit honeycombs described in [2], the maximum difference between the 1D and 2D predictions

TABLE 3-1

TABLE OF EXPRESSIONS FOR THE ELEMENTS b_{ij} of $\vec{B}$

(Note: i refers to a row and j to a column of matrix $\vec{B}$)

i= \ j=	1	2	3	4	5	6
1	1	0	1	1	0	0
2	1	A	ϕ	ϕ^{-1}	0	0
3	-1	a	$-\psi_1$	ψ_2	1	0
4	-1	$-(A + a)$	$\psi_2 \phi$	$-\psi_1 \phi^{-1}$	0	1
5	$\rho_h (1 - \theta)$	$\rho_h (a(1 - \theta) - \theta A)$	$\rho_h \psi_2 (\phi \theta - 1)$	$\rho_h \psi_1 (1 - \phi^{-1} \theta)$	-1	$\rho_h \theta$
6	$\rho_c (1 - \theta)$	$\rho_c (A - a(1 - \theta))$	$\rho_c \psi_1 (\phi - \theta)$	$\rho_c \psi_2 (\theta - \phi^{-1})$	$\rho_c \theta$	-1

Meaning of Symbols:

$\psi_1 = \psi (Pa + 1)^{-1}$; $\psi_2 = \psi (Pa - 1)^{-1}$; $\theta = e^{-(A/a)}$; $\phi = e^{pA}$; $\rho_c = 1 - \epsilon_c$; $\rho_h = 1 - \epsilon_h$

In diffuse case: $\psi = (1 - (1 - \epsilon) P^2/W)$; $a = \frac{1}{2}$

In specular case: $\psi = 1$; $a = 1/(2 \epsilon)$

TABLE 3-2

TABLE OF THE EXPRESSIONS FOR THE ELEMENTS

$\{e_j\}$ OF $\vec{E}$

$e_1 = 1$	$e_4 = \eta$
$e_2 = 0$	$e_5 = -\eta\ (1 + \epsilon_h\ \eta^{-1} - \rho_h\ \theta)$
$e_3 = \eta$	$e_6 = -\eta\ (\ 1 - \rho_c\ \theta)$

See Table 3-1 for definition of θ

$\eta = T_c^4/(T_h^4 - T_c^4)$

TABLE 3-3

SPECULAR ANALYSIS - COMPARISON OF ANALYTICALLY CALCULATED HEAT TRANSFER COEFFICIENTS WITH NUMERICALLY CALCULATED HEAT TRANSFER COEFFICIENTS

ϵ_h	ϵ_c	Aspect ratio	h_T, w/m^2K		Percent Difference
			Analytical	Numerical	
.9	.9	2.4	4.422	4.610	- 4.1
		6.0	2.307	2.719	-15.2
		9.6	1.550	1.976	-21.6
.065	.9	2.4	3.283	3.298	- 0.5
		6.0	1.942	2.152	- 9.8
		9.6	1.373	1.646	-16.6
.065	.065	2.4	2.639	2.594	1.7
		6.0	1.693	1.646	2.9
		9.6	1.246	1.408	-11.5

Conditions: $\Delta T = 7.8^{\circ}C$

$\epsilon = 0.435$

$D = 1.27$ cm

TABLE 3-4

DIFFUSE ANALYSIS - COMPARISON OF ANALYTICALLY CALCULATED HEAT TRANSFER COEFFICIENTS WITH NUMERICALLY CALCULATED HEAT TRANSFER COEFFICIENTS

ϵ_h	ϵ_c	Aspect ratio	h_T, w/m^2K Analytical	h_T, w/m^2K Numerical	Percent Difference
.9	.9	2.4	3.132	3.179	- 1.5
		6.0	1.415	1.493	- 5.2
		9.6	0.907	0.971	- 6.6
.065	.9	2.4	2.632	2.691	- 2.2
		6.0	1.297	1.368	- 5.2
		9.6	0.855	0.920	- 7.1
.065	.065	2.4	2.294	2.322	- 1.2
		6.0	1.209	1.260	- 4.1
		9.6	0.818	0.863	- 5.2

Conditions: $\Delta T = 7.8\ C^o$

$\epsilon_w = 0.435$

$D = 1.27$ cm

of h_T was 9% and the average error was 4.4%, the 2D model always predicting lower h_T's.

Comparison of the various models and experiment is given in the next section.

4. COMPARISON OF EXPERIMENT AND THEORY

4.1 Comparison for Slit Honeycombs

Table 4.1 shows the comparison of the numerical predictions for h_T for the slit honeycombs, with the measured values obtained by Smart [5,2]. The predictions are based on the assumption of diffuse side-wall reflection. Very good agreement is seen to have been obtained, particularly with the 2D treatment. On the basis it was decided that the extra complexity required for the specular analyse was not justified for this geometry.

4.2 Comparison for Hexagonal Honeycombs

4.2.1 Numerical Theory

The comparisons for the measurements on the hexagonal honeycombs with the predictions based on the numerical theory are given in Figures 4-1 through 4-5. Figures 4-1 through 4-3 show the predicted and measured values of h_T plotted against the inverse of aspect ratio for the BB, BS and SS conditions respectively. The BB case shows very good agreement provided one uses the specular model. The maximum error in this case is 7% and the rms error is 3.6%. However in the SB case the specular model appears better at high aspect ratios but at low aspect ratios the diffuse model is superior. A similar trend is to be noted for the SS case in Figure 4-3. Parametric sensitivity studies were undertaken to ascertain whether these trends could be explained on the basis of uncertainties associated with the input parameters to the program, particularly ϵ, ϵ_h and ϵ_c. The conclusion was that the differences could not be explained on this basis. Figure 4-8 shows an interesting

TABLE 4-1

COMPARISON OF SLIT HONEYCOMB PREDICTIONS AND EXPERIMENT

Aspect Ratio	ε, ε_h, ε_c	h_T exp.	h_T 1D	h_T 2D	2D% error	1D - 2D % diff.
			W/m^2K			
5	.13, .06, .06	.874	1.016	.977	11.7	-3.9
10	.13, .06, .06	.783	.818	.789	0.7	-3.5
5	.90, .06, .06	1.38	1.69	1.54	11.5	-9.1
5	.90, .90, .06	1.93	2.10	2.02	4.4	-4.4
5	.90, .90, .90	3.20	2.77	2.73	-14.7	-1.4
3	.13, .06, .06	1.05	1.23	1.18	12.4	-4.2

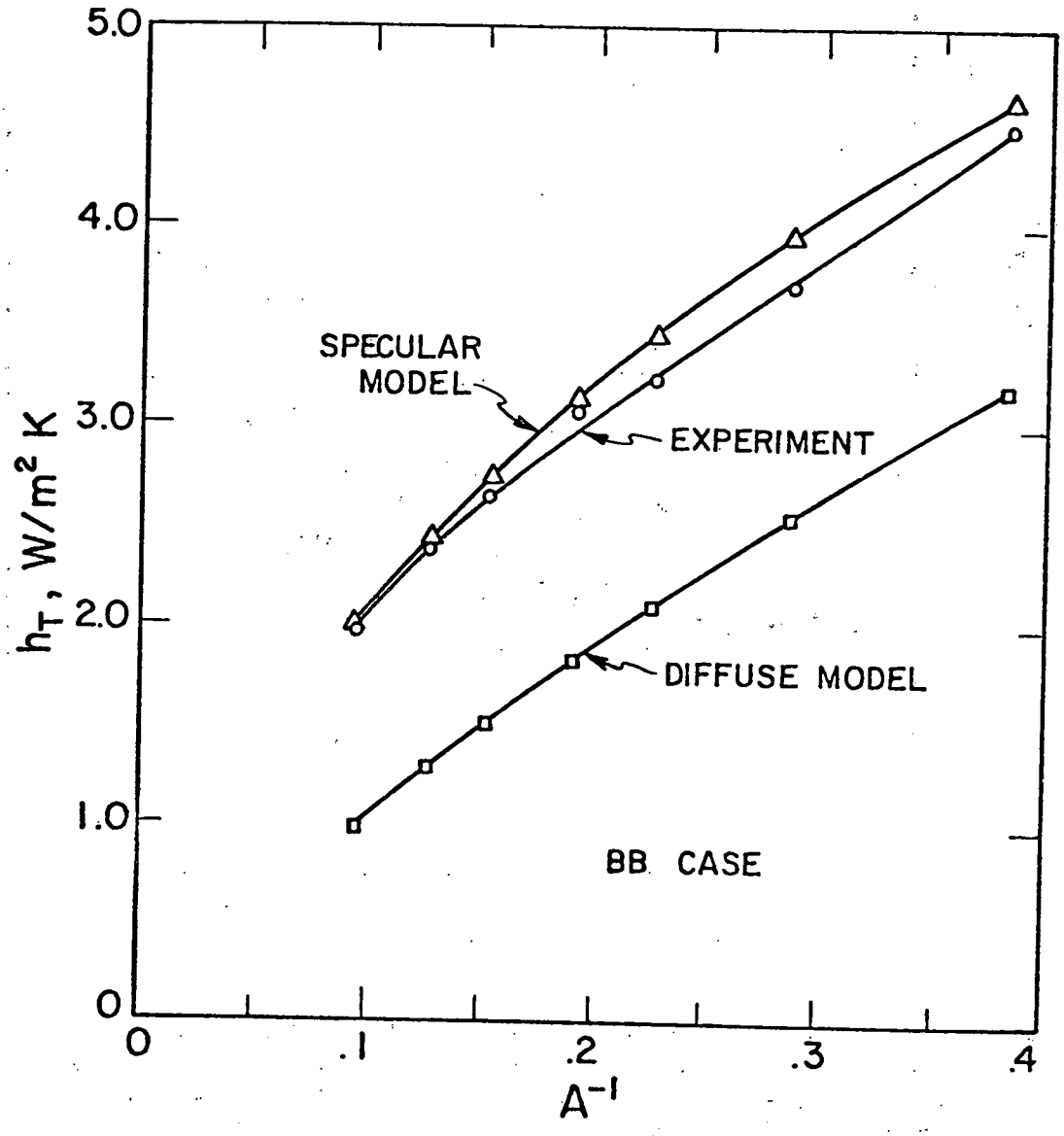

Fig. 4-1 Comparison of h_T measurements with predictions from the "Numerical Theory", for diffuse and specular honeycombs, for high emissivity surfaces both below and above a hexagonal celled honeycomb panel.

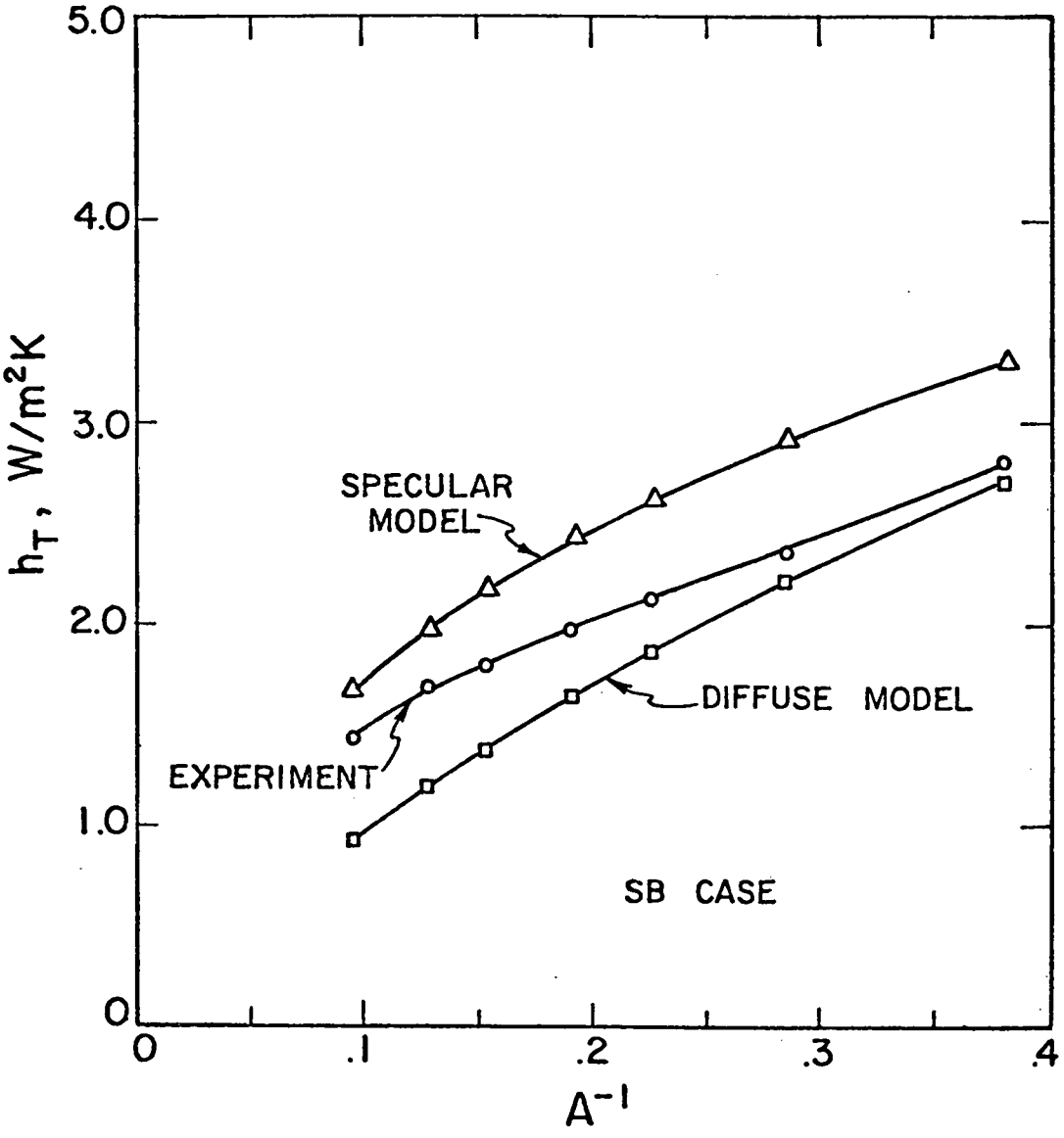

Fig. 4-2 Comparison of h_T measurements with predictions from the "Numerical Theory", for diffuse and specular honeycombs, for a hexagonal-celled honeycomb panel bounded from below by a low emissivity surface and from above by a high emissivity surface.

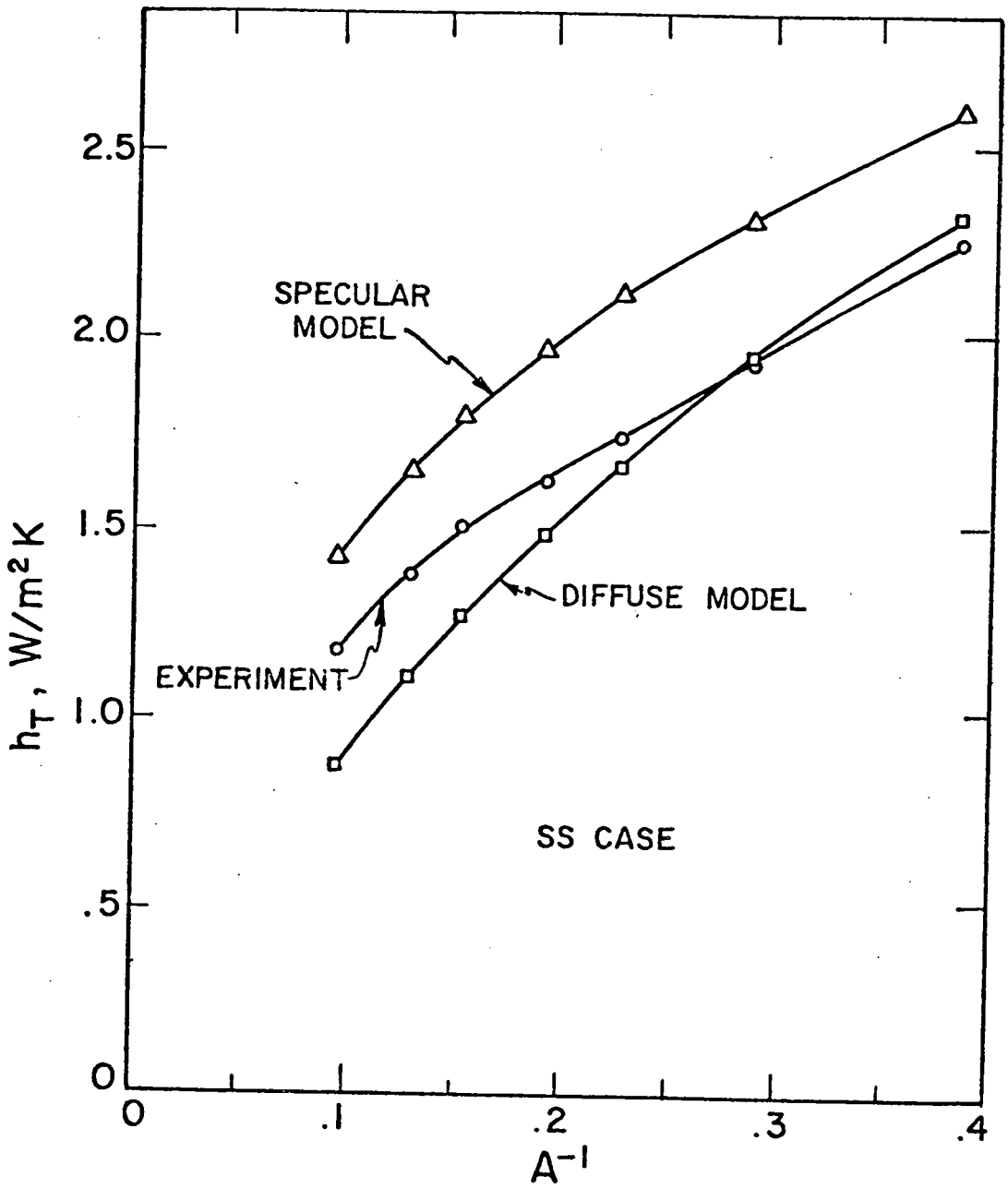

Fig. 4-3 Comparison of h_T measurements with the predictions from the "Numerical Theory", for diffuse and specular honeycombs, for a hexagonal-celled honeycomb panel bounded below and above by low emissivity surfaces.

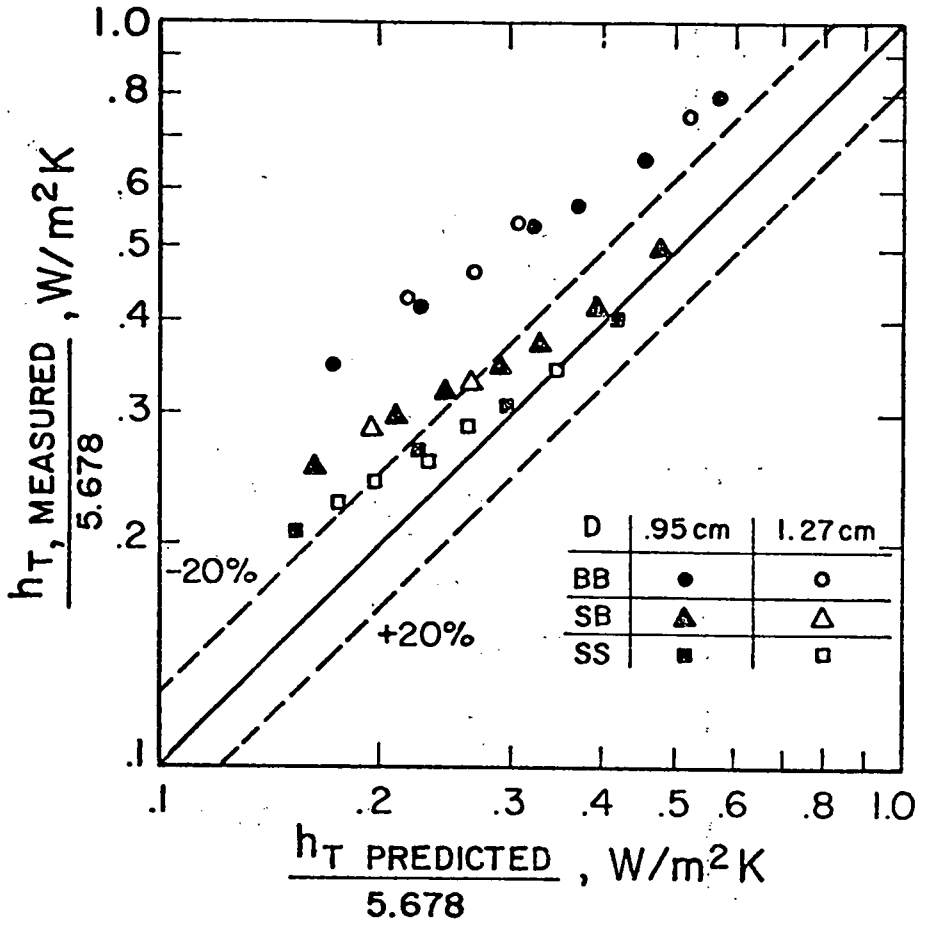

Fig. 4-4 A comparison of measured h_T with values predicted from the "Numerical Theory" in which the honeycomb was assumed to be a diffuse reflector.

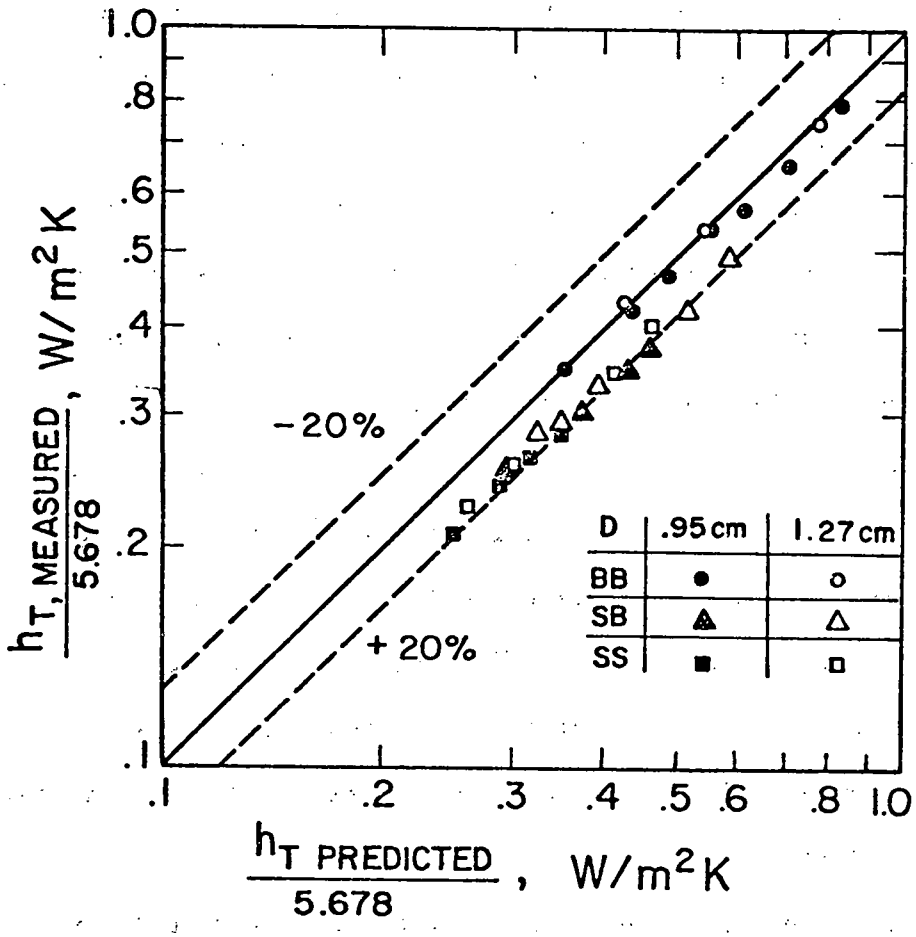

Fig. 4-5 A comparison of measured h_T with values predicted from the "Numerical Theory" in which the honeycomb was assumed to be a specular reflector.

result in this regard, in that only the specular model, and (more importantly), only the measured value of the side-wall emissivity - namely $\epsilon = .435$ - could make the theory predict the measured heat transfer with good accuracy. It is also clear from Figures 4-1 through 4-3 that a theory which was based on partly diffuse and partly specular side-walls could not be expected to predict well since the relative weighting between the two would be expected to be independent of the end-wall emissivities, ϵ_h and ϵ_c, whereas, the figures indicate that the relative weighting (at least in h_T) would have to depend on ϵ_h and ϵ_c, and on A.

Because the agreement with the specular analysis shown in Figure 4-1 is too good to be fortuitous, the side-walls must be concluded to be specular. The lack of agreement in the other two cases is hypothesized to be due to the fact that the side-wall material - Mylar - is not grey, as assumed in the analysis. It is known that Mylar absorbs and emits in bands and is in fact highly non-grey. The non-grey assumption is satisfactory when only a few reflections are involved, however with low emissivities of the end walls the average no. of reflections experienced by an emitted photon before it is absorbed is increased, and the predictions become less satisfactory.

Although the predictions in the specular case are not fully accurate, they are within about 20%, (as can be seen in Figure 4-5) and this is probably sufficient for engineering calculations in solar energy. The added complexity of a non-grey analyses did not therefore, appear justified at this stage.

4.2.2 Analytical Theory

The comparisons with the analytical theory, shown in Figures 4.6

to 4.9, are generally similar in trends to those for the numeric theory although quantitative agreement is not quite as satisfactory. These plots show the predictions of the independent mode method as well as those of the present analysis and hence show the improvements in predictive accuracy due to refinements developed in the present study. In the BB case, agreement is seen to be quite good at aspect ratios of about 5 or less but predictions fall below measurement at high aspect ratios. In the case of SB and BB the diffuse and specular analyses are seen to form bounds between which the data lie. Agreements, although not perfect, is much improved over the independent mode method. The maximum error is again about 20%.

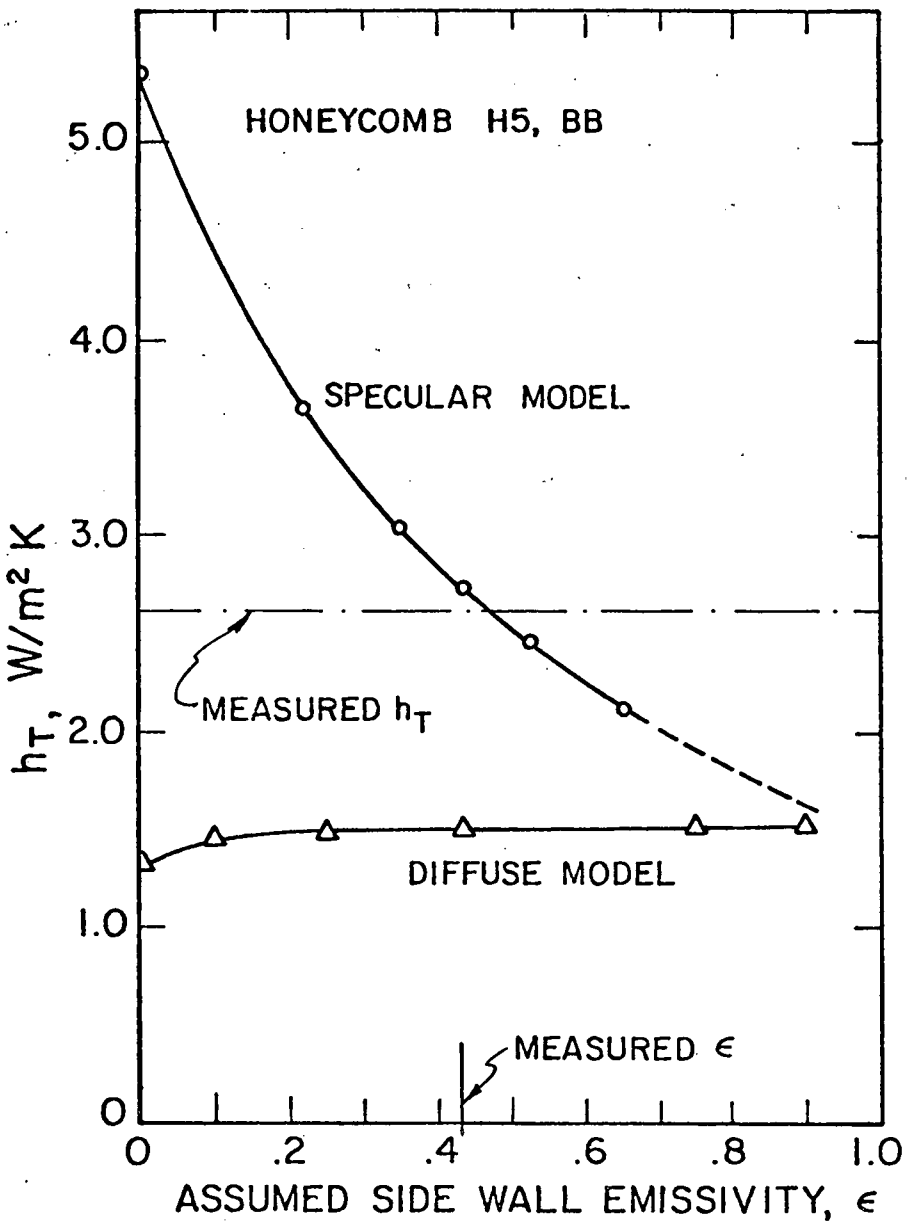

Fig. 4-6 The effect of honeycomb emissivity, ϵ, on the total heat transfer coefficient for two high emissivity bounding surfaces. The incapability of the diffuse side-wall predictions to reproduce the measured h_T for any value of h_T is of particularly note.

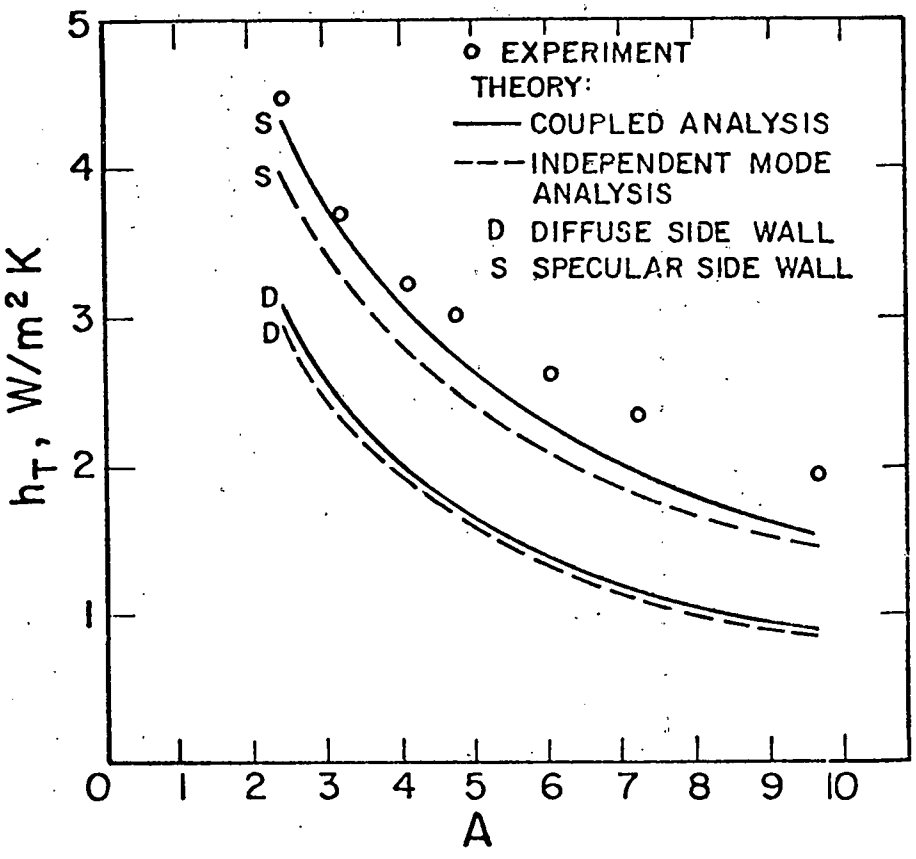

Fig. 4-7 A comparison between measured h_T and predictions of the "Analytical Theory" for both specular and diffuse honeycomb assumptions, and for the independent and coupled mode analyses. The top and bottom plates are of high emissivity (BB case).

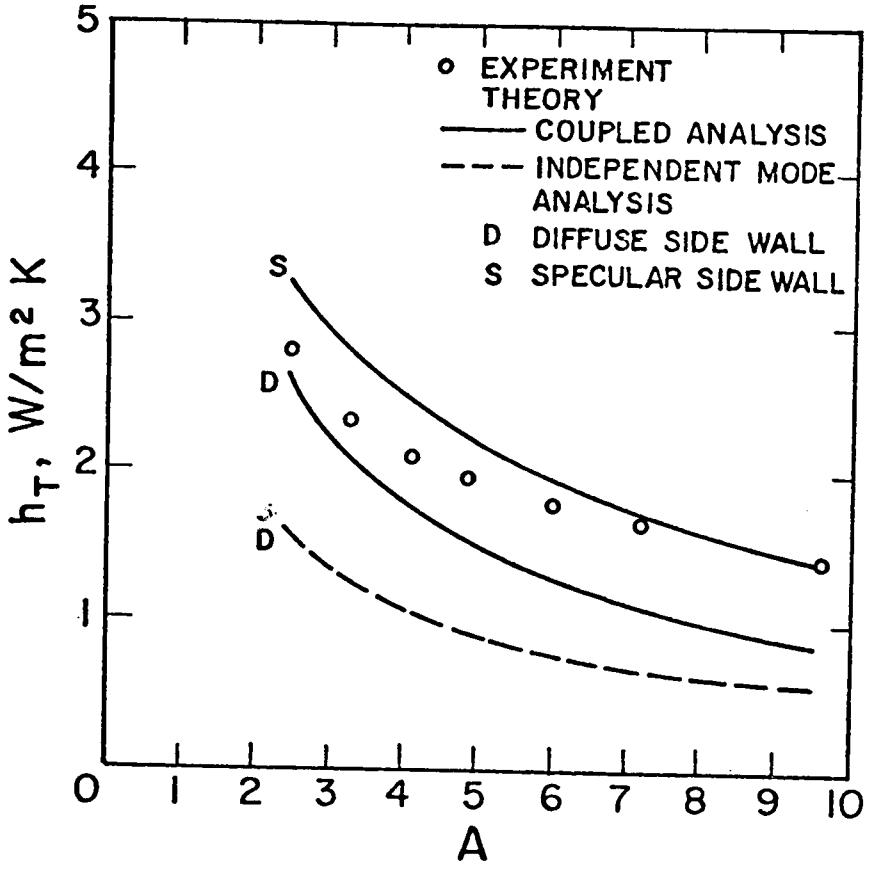

Fig. 4-8 A comparison between measured h_T and predictions of the "Analytical Theory" for both specular and diffuse honeycomb assumptions, and for the independent and coupled mode analyses. The bottom plate has low emissivity and the top plate has high emissivity (SB case).

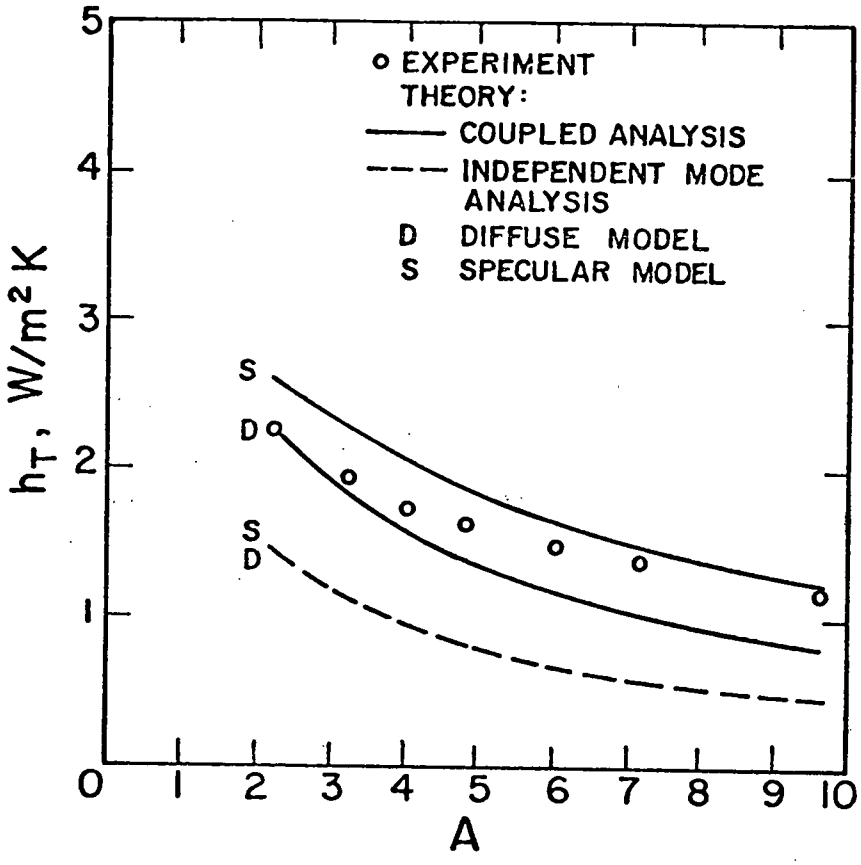

Fig. 4-9 A comparison between measured h_T and predictions of the "Analytical Theory" for both specular and diffuse honeycomb assumptions, and for the independent and coupled mode analyses. Both the bottom and top plates were of low emissivity (S-S case).

5. DISCUSSION OF IMPLICATIONS TO HONEYCOMB COLLECTOR DESIGN

The question of whether honeycombs should be coupled with selective surfaces and/or 'heat-mirrored' glass can now be addressed. Figure 5-1 shows the overall heat transfer coefficient, h_T, plotted against emissivity of honeycomb material ϵ, for a honeycomb having L = 5.07 cm and L/D = 4.8. These curves were calculated assuming specular reflection and based on the analytical method. They neglect conduction in the wall of the honeycomb. A honeycomb of these dimensions will generally suppress free convection in a flat plate collector at the temperatures and angles of inclination of interest. The dependence of h_T on ϵ is shown for 5 combinations of ϵ_h and ϵ_c. The first 3 are the BB, SB, and SS of the experiments. The other two have ϵ_h = .4 and ϵ_c = .88; and ϵ_h = .2 and ϵ_c = .88 respectively.

Consider first the BB case. This corresponds closely to a collector having a black painted absorber plate and a glass cover. A single air layer without a honeycomb in such a collector would have an h_T of about 8.33 W/m^2K.+ A honeycomb fabricated from a high emissivity material - such as a glass honeycomb, would yield an overall h_T of about 1.8 W/m^2K, thus yielding a factor of 4.5 reduction in h_T. If a plastic honeycomb fabricated from Mylar film of thickness the same as that of the present study, the value of ϵ is about .43 so that h_T becomes 2.6 and a reduction of 3.2 is achieved. If on the other hand the honeycomb material has an emissivity of ϵ = .14, which is representative of teflon film in .012 mm (.0005 inches) thickness, h_T will be 4.3, and the reduction is only a factor of two. Thus a honeycomb with as high an emissivity as possible is desirable in the BB case. If a high emissivity

+ based on an air layer width, L, of about 1 cm.

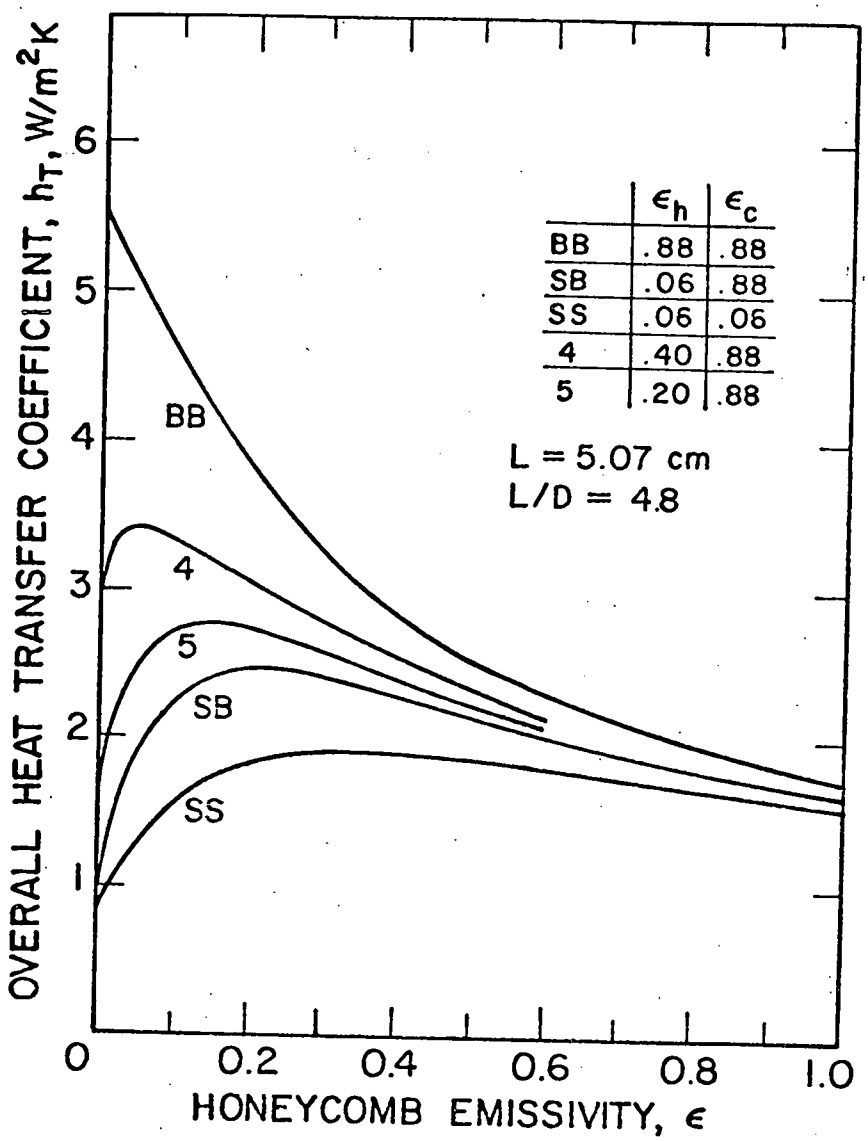

Fig. 5-1 The dependence of overall heat transfer coefficient on emissivity of the honeycomb material for panels bounded below and above by plates of various emissivities. The predictions are from the "Analytical Theory" using the specular side wall approximation, with a cell aspect ratio of 4.8.

honeycomb material is used, the value of h_T is relatively insensitive to ϵ_c and ϵ_h.

In the case of thin teflon film mentioned above, the honeycomb is largely giving only convection suppression. However, teflon may still be an attractive option for honeycombs because of its UV stability and high temperature resistance, (although its cost is also high). Because it is expensive, it must be used in thin films and this largely accounts for its low emissivity. A combination of a thin teflon film and a selective surface therefore may be of interest since it can obtain its convection suppression from the honeycomb and the radiant suppression from the selective surface. The curve in this case should fall between the SB curve and curve 5 since most selective surfaces have an emissivity between .06 and .2. In this instance the values should be compared to a single air layer with a selective surface and no honeycomb, for which h_T is about 4 W/m^2K for $\epsilon_h = .2$, and 3 W/m^2K for $\epsilon_h = .06$. It is seen that the reduction in h_T due to the honeycomb in case 5 is from 4 to 2.7 W/m^2K or only 33%, and in case SB the corresponding reduction is only 25%. In neither case is the resulting h_T as low as that obtainable from a honeycomb of high ϵ and no selective surface. To obtain the desired low value of h_T by a combination selective surface and honeycomb, it is seen that very low values of ϵ are required, (of the order of .01). If these are achieved, values of h_T of order of 1.2 W/m^2K are predicted.

Very low h_T's are predicted for the SS with $\epsilon = .14$ case although this would have to incorporate a very good selective and an excellent heat mirror. The fact that at $\epsilon = 1$, all the curves collapse to very nearly the same h_T indicates that selective surfaces are of

virtually no value if a honeycomb of high ϵ is already in place.

An interesting feature of these plots is the fact that in cases 5, SB and SS there exists an ϵ which maximizes h_T. This result is a consequence of the radiant-conductive coupling: at the two local minimae, namely $\epsilon = 0$ and $\epsilon = 1$, the coupling is either non-existent (the $\epsilon = 0$ case), or, because both the radiative and conductive fields attempt to establish very similar temperature fields, it is small (the $\epsilon = 1$ case).

6. CONCLUSIONS

1. The effect of bounding plate emissivities on the critical Rayleigh number (i.e. convection suppression abilities) of hexagonal honeycombs is very slight. It is maximum when the two bounding surfaces have very different emissivities and for honeycombs of high aspect ratio.

2. Theoretical methods, (both numerical and analytic) have been developed which predict the overall heat transfer across hexagonal and slit-type honeycombs in the stagnant air condition to within about 20% as compared to measurements. These methods take into account the important coupling between the radiative and conductive modes of heat transfer.

3. From the predictions of these methods it is concluded that the combination of a selective surface and a honeycomb gives disappointingly low advantages over using either one of them singly. Thus, when the honeycomb wall emissivity is high, ($\epsilon \approx .9$) very little advantage is to be gained by having a selective surface; if the wall emissivity is moderate ($\epsilon \approx .5$), only an additional 25 to 33% reduction in heat transfer is obtained due to use of a honeycomb, if a selective surface is already in place. Only for wall emissivities of the order of .01 does the combination appear promising.

7. LIST OF REFERENCES

1. Hollands, K.G.T., Raithby, G.D., and Unny, T.E., "Studies on Methods of Reducing Heat Losses from Flat-Plate Solar Collectors", University of Waterloo Research Institute Report, under Contract No. E(11-1)-2597, June, 1976, (N.T.I.S.+ No C00-2597-2).

2. Hollands, K.G.T., Raithby, G.D., and Unny, T.E., "Methods for Reducing Heat Losses from Flat Plate Solar Collectors, Phase II", University of Waterloo Research Institute Report, under Contract No. EY-76-C-02-2597, March 1978, (N.T.I.S.+ No. C00-2597-4).

3. Marshall, K.N., Wedel, R.K., Dammanne. R.E., "Development of Plastic Honeycomb Flat Plate Solar Collectors", Lockheed Palo Alto Research Labs Report No. LMSC/D 462879, prepared under ERDA contract E (04-3) -1081, April, 1976.

4. Hollands, K.G.T., "Honeycomb devices in Flat Plate Solar Collectors", Solar Energy, 9, p. 159, (1965).

5. Smart, D.R. "Convection Suppression and Heat Transfer in Air Constrained by Slit Type Honeycomb with Application to Flat Plate Solar Collector Design", M.A.Sc. Thesis, Department of Mechanical Engineering, University of Waterloo, Ontario, Canada (1978).

6. Hottel, H.C., Keller, J.D., "Effect of Reradiation on Heat Transfer in Furnaces and Through Openings", Trans. ASME, Vol. 55, pp. 39-49, 1933.

7. Edwards, D.K., Tobin, R.D,"Effect of Polarization on Radiant Heat Transfer Through Long Passages", J. Heat Transfer, Vol. 89, pp. 132-138, 1967.

8. Tien, C.L. and Yuen, W.W., "Radiation Characteristics of Honeycomb Solar Collectors", Int. J. Heat Mass Transfer, 18, pp. pp. 1409-1413, (1975).

9. Perlmutter, M. and Siegel, R., "Effect of Specularly Reflecting Gray Surface on Thermal Radiation through a Tube and its Heated Wall", J.Heat Transfer, 85, 1, pp 55-62, 1963.

10. Buchberg, H. and Edwards, D.K., "Design Considerations for Solar Collectors with Cylindrical Glass Honeycombs", Solar Energy, Vol. 18, pp 193-203, 1976.

11. Felland, J.R. and Edwards, D.K., "Solar Infrared Radiation Properties of Parallel-Plate Honeycombs", J.Energy, 2, No. 5, pp 309-317, 1978.

+ National Technical Information Services, U.S. Department of Commerce, 5285 Port Royal Rd., Springfield Va, 22161, USA

12. Hollands, K.G.T., "Natural Convection in Horizontal Thin-Walled Honeycomb Panels", J. Heat Transfer, Vol. 95, pp 439-444, (1973).

13. Hollands, K.G.T., Konicek, L., "Experimental Study of the Stability of Differentially Heated Inclined Air Layers", Int. J.Heat Mass Transfer 16, pp. 1467-1476 (1973).

14. Ruth, D.W., "On Free Convection by Longitudinal Rolls in Inclined Infinite Air Layers Heated from Below", Ph.D. thesis, Dept. Mechanical Engineering, University of Waterloo, 1977.

15. Cane, R.L.D., Hollands, K.G.T., Raithby, G.D., Unny, T.E., "Free Convection Heat Transfer Across Inclined Honeycomb Panels", Journal of Heat Transfer, 99, No. 1, pp. 86-91, 1977.

16. Sun, W.M., "Effect of Arbitrary Wall Conduction and Radiation on Free Convection in a Cylinder", Ph.D. Thesis, University of California, Los Angeles, (1970), (see also Sun. W.M. and Edwards, D.K. "Natural Convection in Cells of Finite Conductivity Walls Heated from Below", 4th Int. Heat Transf. Conf., Versailles, France, Elsevier Pub. Co., Amsterdam, Paper NC, 2.3, (1971).).

17. Wilkinson, R.G., "Radiative-Conductive Heat Transfer Through A Honeycomb Panel", M.A.Sc. Thesis, Dept. Mechanical Engineering, University of Waterloo, 1979.

18. Russel, F.B., "The Prediction of Stagnant Air Heat Transfer Across Honeycombs Employing Numerical Methods", M.A.Sc. Thesis, Dept. Mechanical Engineering, University of Waterloo, 1979.

19. Siegel, R. and Howell, J.R., Thermal Radiation Heat Transfer, McGraw-Hill, New York (1972), p. 265.

8. NOMENCLATURE

Note: The meaning of symbols in Table 3-1 and 3-2 are specific to those tables and are given at the bottom of those tables.

A	aspect ratio of honeycomb cell, $A = L/D$.
$A_{c,g}, A_g$	cross-sectional area of the gas core in a single honeycomb cell
$A_{c,s}, A_s$	cross-sectional area of the solid shell of the honeycomb material in a single honeycomb cell
$\vec{B}$	a 6 x 6 coefficient matrix, used in equation 3-7, with elements $\{b_{ij}\}$
$\{b_{ij}\}$	elements of the matrix $\vec{B}$, tabulated in Table 3-1
b	a constant chosen so as to satisfy equations A-24 and A-25
BB	see Table 2-1
D	effective honeycomb cell diameter; for slit honeycomb D = spacing between partitions; for hexagonal honeycombs, $D = (4A_g/\pi)^{\frac{1}{2}}$
$\vec{E}$	a row vector used in equation 3-7, with elements $\{e_j\}$
$\{e_j\}$	elements of the row vector $\vec{E}$, tabulated in Table 3-2
$\overline{F}$	Hottel and Keller radiant interchange factor, defined in equation (1-6)
$\overline{F}'$	Hollands modified $\overline{F}$ to account for non-black end walls, defined in equation (1-8)
F^n_{i-j}	diffuse (for n=1) or specular (for n=2) radiant form factor from i^{th} to j^{th} surface
g	gravitational acceleration
h	heat transfer coefficient, for heat flow between the plates

h_c = k_e/L

h_T the value of h for combined radiation and conduction between the plates if the air is stagnant

$h_{T,c}$ the value of h for combined radiative conductive and convective heat transfer between the plates: $h_{T,c} = h_T$ in the absence of fluid motion

h_r $h_T - h_c$

J_i for n = 1, J_i is the i^{th} surface radiosity; for n = 2, J_i represents the radiant flux emitted from the i^{th} surface

k_e effective thermal conductivity of honeycomb and gas, defined by equation (1-4)

k_g thermal conductivity of the gas (air) within the honeycomb cells

k_s thermal conductivity of the material from which the honeycomb is fabricated

L spacing between the plates, or depth of the honeycomb panel; see Figure 1-1

n n = 1 for diffusely reflecting honeycomb; n = 2 for specular reflecting honeycomb

Nu Nusselt number. See equation (1-5)

P in equation 1-2, P represents the pressure of the air; otherwise it is defined by equation 3-4.

Pr Prandtl number

$q_{c,w}$ net heat flux conducted into honeycomb side wall

$q_{r,w}$ net heat flux radiated into honeycomb side wall

q_r radiant flux across the honeycomb panel, assuming heat conduction and radiation modes are decoupled

r	radial co-ordinate in cylindrical co-ordinate system, see Figure A-1 and A-2.
R	= D/2
$\bar{R}$	gas constant for air
Ra	Rayleigh number; $Ra = g\beta(T_h - T_c)L^3/\nu\lambda$
Ra_c	critical Rayleigh number for the initiation of convection
T	absolute local temperature of gas or solid
$\bar{T}_g, \bar{T}_s$	average temperature in gaseous and solid portions of honeycomb cell, respectively
$\bar{T}_{g,s}$	see equation A-22
T_c	temperature of the upper cool plate, absolute
T_h	temperature of the lower hot plate, absolute
T_w	temperature of honeycomb cell side-wall, absolute
t	semi-thickness of honeycomb material
SB	see Table 2-1
SS	see Table 2-1
W	constant in the "Analytical Theory", defined by equation (3-5)
x, x_i	$\lvert z' z\rvert/2R$ and $\lvert z'-z\rvert/(2R(i+1))$ respectively
z, z'	co-ordinates, see Figures A-1 and A-2.

Greek Letters

β	thermal expansion coefficient for gas in honeycomb panel
β_i	dimensionless radiosity, see equation A-33
γ_j	constants in equation (3-3) that are defined by the vector equation, (3-7).j = 1, 2, 3, 4, 5, 6
$\vec{\gamma}$	the row vector with elements γ_j
γ'	the column vector with elements γ_j. $\vec{\gamma}'$ is the transpose of $\vec{\gamma}$
δ_{2n}	= 1 for n = 1; = 0 for n = 2
ε	emissivity of the honeycomb wall
ε_i	emissivity of the upper cooled plate; see Figure 1-1
ε_h	emissivity of the lower heated plate, see Figure 1-1
η	$= z^1/2R$
θ	angle of inclination of the honeycomb panel, measured from the horizontal; see Figure 1-1
ξ	z/2R
λ	thermal diffusivity of gas contained in honeycomb panel
μ	dynamic viscosity of gas contained in honeycomb panel
ν	kinematic viscosity of gas contained in honeycomb panel
ρ	reflectivity of honeycomb material
ρ	effective reflectivity of honeycomb; $\rho_e = \rho + \tau$
σ	Stefan Boltzmann constant
τ	trasnmissivity of honeycomb material
ϕ	dimensionless temperature, see equation A-32
γ_i	see equation A-34

9. LIST OF CONTRIBUTING PERSONNEL

Principal Investigator:

K.G.T. Hollands, Professor, Department of Mechanical Engineering

Faculty Associates:

G.D. Raithby, Professor, Department of Mechanical Engineering.

Graduate Students:

F.B. Russell, Research Assistant, Department of Mechanical Engineering

R.G. Wilkinson, Research Assistant, Department of Mechanical Engineering.

Lab Technician:

M. Kaptein, Thermal Engineering Lab., Department of Mechanical Engineering.

10. LIST OF PUBLICATIONS AND PAPERS ISSUED DURING THE TOTAL CONTRACT PERIOD

1. Cane, R.L.D., Hollands, K.G.T., Raithby, G.D., Unny, T.E., "Free Convection Heat Transfer Across Inclined Honeycomb Panels", Journal of Heat Transfer, 99, No. 1, pp. 86-91, Feb. 1977.

2. Hollands, K.G.T., Unny, T.E., Raithby, G.D., Konicek, L., "Free Convection Across Inclined Air Layers", J. Heat Transfer 98, No. 2, pp. 189-193 (1976).

3. Raithby, G.D., Hollands, K.G.T., and Unny, T.E., "Free Convection Heat Transfer Across Fluid Layers of Large Aspect Ratios", J. Heat Transfer, 99, No. 2, pp. 287-293, (1977).

4. Sibbitt, B.E., Hollands, K.G.T., "Radiant Transmittance of V-Corrugated Transparent sheets, With Application to Solar Collectors," ASME Paper No., 76-WA-Sol-1, W.A. meeting of ASME, New York, Dec. 1976.

5. ElShirbeny, S.M., Hollands, K.G.T. and Raithby, G.D., "Free Convection across Inclined Air Layers with one Surface V-corrugated", Journal of Heat Transfer, 100, No. 3, pp. 410-415, (1978).

6. Hollands, K.G.T. "Dimensional Relations for Free Convective Heat Transfer in Flat-Plate Collectors". Proceedings of the 1978 Annual Meeting of the American Section of the International Solar Energy Society, 2.1, pp. 207-213, Pergamon Press, (1978).

7. Smart, D.R., Hollands, K.G.T., Raithby, G.D., "Free Convective Heat Transfer across Rectangular-celled, Diathermous Honeycombs", submitted to Journal of Heat Transfer, March, 1979.

APPENDIX

Outline of Theory Used to Predict the Stagnant Air Heat Transfer

Note: The hexagonal-type honeycomb theory will be outlined only. The slit-type honeycomb theory follows a very similar development. Complete details for both are given in [17] and [18].

A-1 Model

The heat transfer analysis across the honeycomb is performed on a typical honeycomb cell which is approximated by the circular-cylinder shell shown in Figure A-1. The core inside the shell contains the gas (air). The lateral outer boundaries are adiabatic while both the gas and solid are isothermal at T_h and T_c at the bottom and top faces respectively. Heat transfer is by conduction only in the solid part and by conduction and radiation in the gaseous part. The gas is transparent to thermal radiation and the surface at $z = R$ is strongly opaque to thermal radiation so that all heat transfer between the radiant and conductive fields occurs at the surface $r = R$. Figure A-2 sketches the radiant enclosure problem, the gaseous inner cylinder constituting the radiant enclosure. The lower and upper face are diffuse grey emitters and reflectors and have emissivities ϵ_h and ϵ_c respectively. The side-walls are opaque and grey with emissivity ϵ; the temperature and heat flux at these side-walls are such as to be compatible with the conductive heat transfer. In the analytical theory the radiosity was assumed to be uniform over the lower and upper faces; this was not assumed for the numerical theory. The difference due to this assumption is expected to

be slight. The following development will, for simplicity, make this uniform radiosity assumption.

A-2 Governing Equations

The equations governing the radiant transfer in the inner cylinder (Figure A-2) are:

$$J_w(z) = \epsilon\, \sigma\, T_w^4(z) + (1 - \epsilon)\, \{J_h\, F^n_{dw-h} + J_c\, F^n_{dw-c} + \int_o^L J_w(z') \cdot \frac{d\, F^n_{dw-dw'}}{dz'}\, dz'\}\, \delta_{2n} \qquad \text{A-1}$$

$$J_h = \epsilon_h\, \sigma\, T_h^4 + (1 - \epsilon_h)\, \{J_c\, F^n_{h-c} + \int_o^L J_w(z') \cdot \frac{d\, F^n_{h-dw'}}{dz'}\, dz'\}\, \delta_{2n} \qquad \text{A-2}$$

$$J_c = \epsilon_c\, \sigma\, T_c^4 + (1 - \epsilon_c)\, \{J_h\, F^n_{c-h} + \int_o^L J_w(z') \cdot \frac{d\, F^n_{c-dw'}}{dz'}\, dz'\}\, \delta_{2n} \qquad \text{A-3}$$

In these equations n represnets an index which is defined as equal to unity (n=1) if the side-walls are diffuse, and as equal to two (n=2) if the side-walls are specular. Thus the equations as written are general and can apply to either situation. The quantity F^n_{a-b} represents either the diffuse or specular radiant form factor between a and b, depending on the value of n. The quantity δ_{2n} is given by:

$$\delta_{2n} = 1 \qquad n = 1$$

$$\delta_{2n} = 0 \qquad n = 2$$

The symbol T represents temperature and J represents the radiosity if n=1 and it represents the net, non-specularly reflected radiant flux leaving the surface, if n=2. Subscripts h, c and w on J, T and F^n represent the lower hot surface, the upper cold surface and the side-walls

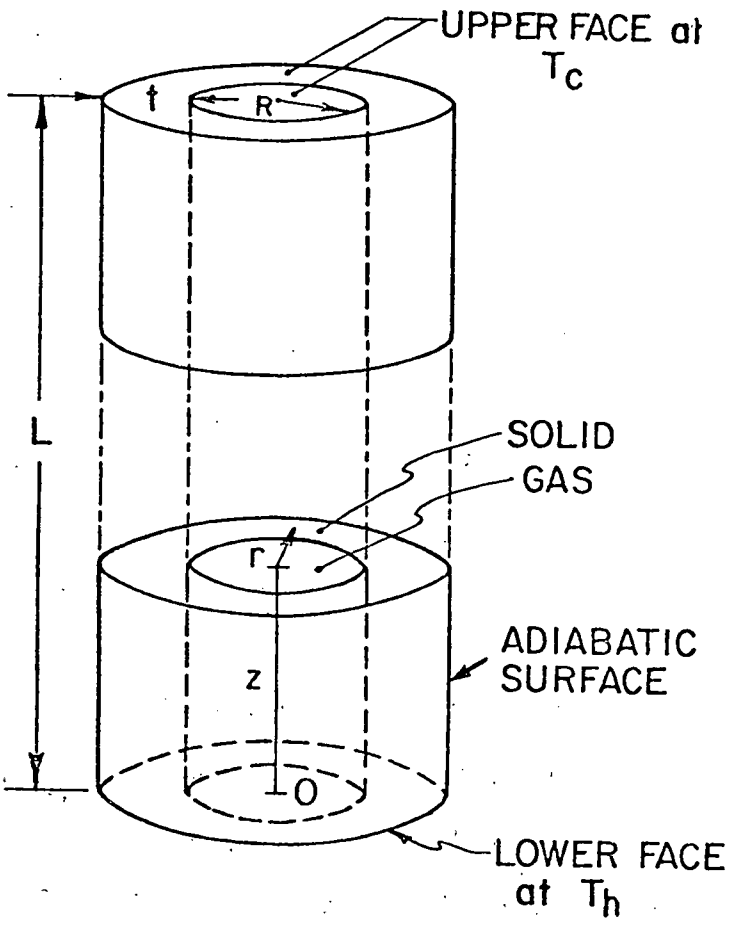

Fig. A-1 A single honeycomb cell idealized as a solid cylindrical shell comprised of honeycomb material and a gaseous core.

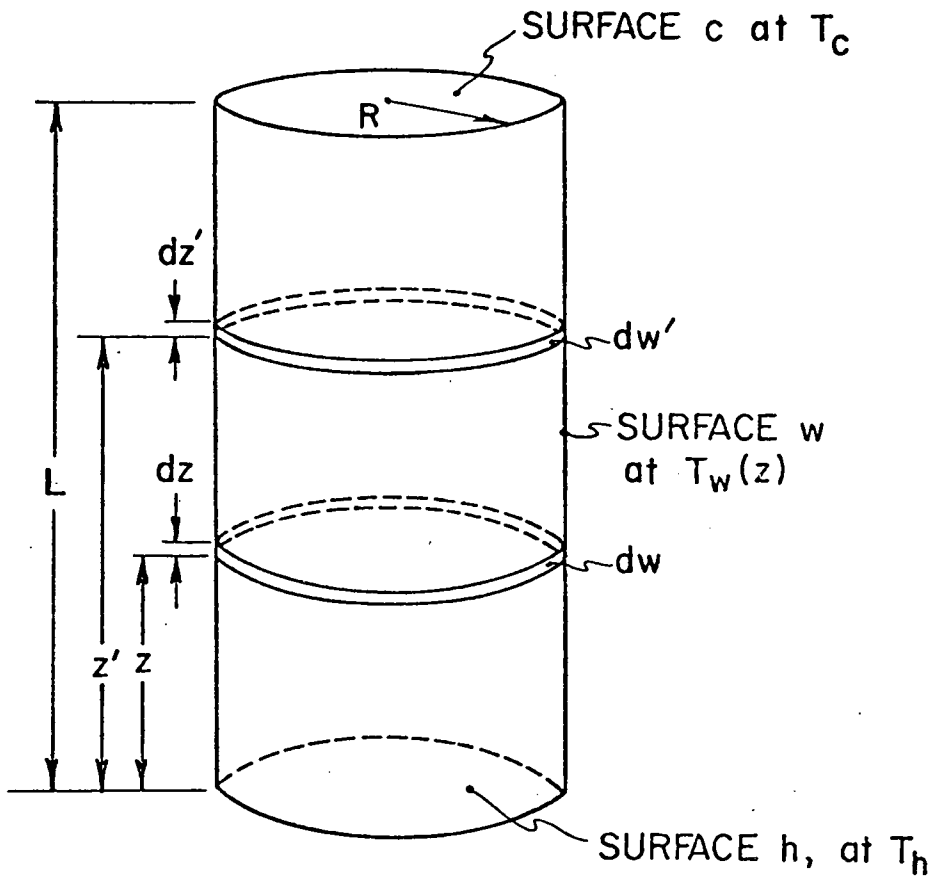

Fig. A-2 A schematic giving nomenclature for the radiant enclosure analysis, detailing the inner of the two cylinders in Fig. A-1.

respectively. Subscripts dw and dw' on F^n denote elemental rings on the side-walls as shown in Figure A-2.

The expressions for the key radiant form factors are

$$\frac{d\,F^1_{dw-dw'}}{dz'} = \frac{1}{2R}\left[\,1 - \frac{2x^3 + 3x}{2(x^2+1)^{3/2}}\,\right] \qquad \text{A-4}$$

and

$$\frac{d\,F^2_{dw-dw'}}{dz'} = \frac{1}{2R}\sum_{i=0}^{\infty}\frac{(1-\epsilon)^i}{i+1}\left(1 - \frac{2x_i^3 + 3x_i}{2(x_i^2+1)^{3/2}}\right) \qquad \text{A-5}$$

where $x = |z' - z|/2R$ and $x_i = x/(i+1)$. The other radiant form factors for the enclosure appearing in equations A-1 to A-3 can be readily derived from these using flux algebra. The full set of expressions are given in [17] and [18].

The equation governing the conductive transfer in both the solid and the gas is:

$$\frac{1}{r}\frac{\partial}{\partial r}\left(r\frac{\partial T}{\partial r}\right) + \frac{\partial^2 T}{\partial z^2} = 0 \qquad \text{A-6}$$

The symbol T represents the local temperature, T(r,z). The boundary conditions on this equation are:

at $r = R + t$ $\qquad \frac{\partial T}{\partial r} = 0$ $\qquad$ A-7

at $r = 0$ $\qquad \frac{\partial T}{\partial r} = 0$ $\qquad$ A-8

at $z = 0$ $\qquad T = T_h$ $\qquad$ A-9

at $z = L$ $\qquad T = T_c$ $\qquad$ A-10

The solutions in the solid and gas are coupled at the interface

through the requirement that temperature be continuous, and that the radiant and conductive transfer at the interface satisfy energy conservation. The radiant flux out of this surface is:

$$q_{r,w} = \epsilon(\sigma T_w^4 - J_h F^n_{dw-h} - J_c F^n_{dw-c} - \int_o^L J_w(z') \frac{d F^n_{dw-dw'}}{dz'} dz') \qquad A-11$$

The net conductive flux in the inward direction at the interface is

$$q_{c,w} = k_s \left.\frac{\partial T}{\partial r}\right|_{r=R^+} - k_g \left.\frac{\partial T}{\partial r}\right|_{r=R^-} \qquad A-12$$

where k_s and k_g are thermal conductivities of the solid and gas respectively and R^+ indicates that the derivative is taken on the solid side of the interface, and R^- that it is taken on the gaseous side. An energy balance at the interface gives:

$$q_{r,w} = q_{c,w} \qquad A-13$$

Also, for continuity of temperature:

$$T_w(z) = T(R,z) \qquad A-14$$

Equations A-1 to A-14 and the subsidiary set of reciprocity relations for the radiant form factors form a complete set of equations which can be solved for $T(r,z)$, $T_w(z)$, $J_w(z)$, J_c and J_h. Once these are obtained, the total heat transfer coefficient h_T, across the cylinder from T_h to T_c can be determined from the following relations

$$h_T = (Q_c + Q_r)/(A_g + A_s)(T_h - T_c) \qquad A-15$$

where

$$Q_c = k_g \int_o^R \left(-\frac{\partial T}{\partial z}\right)_{z=0} 2\pi r\, dr + k_s \int_R^{R+t} \left(-\frac{\partial T}{\partial z}\right)_{z=0} 2\pi r\, dr \qquad \text{A-16}$$

and

$$Q_r = A_g \frac{\epsilon_h}{1-\epsilon_h} (\sigma T_h^4 - J_h) \qquad \text{A-17}$$

A-3 The 1D Approximation

Taking an area weighted average of equation A-4 over each of the gaseous and solid regions and using equations A-5 and A-6 yields

$$\left.\frac{\partial T}{\partial r}\right|_{R^-} = -\frac{A_g}{2\pi R} \frac{d^2 \bar{T}_g(z)}{dz^2} \qquad \text{A-18}$$

$$\left.\frac{\partial T}{\partial r}\right|_{R^+} = \frac{A_s}{2\pi R} \frac{d^2 \bar{T}_s(z)}{dz^2} \qquad \text{A-19}$$

where $\bar{T}_s(z)$ and $\bar{T}_g(z)$ represent respectively the area weighted average of $T(r,z)$ over the solid and gaseous regions respectively and A_s and A_g represent the respective cross-sectional areas of these regions, i.e. $A_s = \pi R^2$ and $A_g = \pi(R + t)^2 - R^2$. Combining A-18 and A-19 with A-12 and A-13 yields

$$\frac{k_e (A_g + A_s)}{2\pi R} \frac{d^2 \bar{T}_{g,s}(z)}{dz^2} = q_{r,w} \qquad \text{A-20}$$

where $q_{r,w}$ is given by A-11 and where

$$\bar{T}_{g,s}(z) = \frac{k_s A_s \bar{T}_s(z) + k_g A_g \bar{T}_g(z)}{k_s A_s + k_g A_g} \qquad \text{A-21}$$

and k_e, the effective thermal conductivity, is given by

$$k_e = \frac{A_s k_s + A_g k_g}{A_s + A_g} \qquad \text{A-22}$$

The 1D approximation assumes that, to a reasonable approximation for the purposes of radiant calculations, the wall temperature can be taken as equal to the weighted mean gas-solid temperature:

$$T_w(z) = \bar{T}_{g,s}(z) \qquad \text{A-23}$$

Equations A-1,2,3,4,5,9,10,11,20 and 23 now form a complete set and equation A-6 need not be solved. Once that set has been solved for $T_w(z)$, $J_w(z)$, J_c and J_h, then h_T may still be found from A-16 and A-18, but calculating Q_c from:

$$Q_c = k_e A_{g,s}\left(-\frac{d T_w(z)}{dz}\right) \qquad \text{A-24}$$

A-4 The Exponential Kernel Approximation

If the form factor expressions in A-4 and A-5 can be approximated with satisfactory accuracy by exponential functions then, under certain circumstances, analytical expressions can be derived for the solution to the equations. The requirement is that equations A-4 and A-5 can be approximated by

$$\frac{d F^n_{dw-dw'}}{dz'} \approx \frac{1}{2R} e^{-bx} \qquad \text{A-24}$$

where b is a constant, whose value may depend upon n. Once the decisions to approximate according to A-24 is made, the value of b should be fixed so as to ensure that the expression obeys the necessary energy conservation law:

$$\epsilon^{n-1} \int_{z'=-\infty}^{z'=\infty} d\, F^n_{dw-dw'} = 1 \qquad \text{A-25}$$

(This expression is derived on the basis of an infinite cylinder but it should also be satisfied by a finite cylinder to ensure that F_{dw-h} and F_{dw-c} are also consistent with an overall radiant balance). The equation simply states that any radiant energy leaving dw must eventually be absorbed somewhere on the walls. For n=1 equations A-24 and A-25 combine to give b=2; for n=2 they give b=2ε. Reference [19] gives a comparison of the exact and approximate expressions for $d\, F^n_{dw-dw'}/dz$, for n=1, with b=2. The fit was found to be very good. For n=2 the fit is not found to be quite so satisfactory.

A-5 Analytical Solution for Nonconducting Case

If $k_a = 0$ and the product $k_w t$ is zero (so that $k_e = 0$), the plane at r = R becomes adiabatic. The solution to the remaining purely radiant problem will now be outlined using the exponential kernel approximation. The method will assume $\epsilon_h = \epsilon_c = 1$, the results to be generalized to other values afterwards. This makes $J_h = \sigma T_h^4$ and $J_c = \sigma T_c^4$. Also since $q_{c,w} = 0$, $q_{r,w} = 0$ and equation A-11 simplifies. The procedure is different for n=1 from that for n=2. For n=1, A-11 with $q_{r,w} = 0$ is combined with equation A-1 to show that $J_w = \sigma T_w^4$. Substituting this into equation A-11 and using A-24 for the form factors there results

$$T_w^4(\xi) = T_h^4 \frac{e^{-b\xi}}{2} + T_c^4 \frac{e^{-b(A-\xi)}}{2} + \epsilon_w^{(n-1)} \int_0^A T_w^4(\eta)\, e^{-b|\xi-\eta|} d\eta \qquad \text{A-26}$$

where $\xi = z/2R$ and $\eta = z'/2R$. The same equation is obtained for the n=2 case by noting that in this case A-1 gives simply $J_w = \epsilon(\sigma T_w^4)$, and by substituting this result into A-11 with $q_{r,w} = 0$. This integral equation

may be converted to a simple differential equation by differentiating it twice and combining the resulting equation with the original equation. The result is

$$\frac{d^2 T_w^4}{d \xi^2} = 0 \qquad \text{A-27}$$

with solution

$$T_w^4 = C_1 + C_2 \xi \qquad \text{A-28}$$

The constants C_1 and C_2 are evaluated by substitution back into A-26. The resulting expression for $T_w(\xi)$ is:

$$\frac{T_h^4 - T_w(\xi)}{T_h^4 - T_c^4} = \frac{1}{2(\epsilon^{n-1} A + 1)} + \frac{\epsilon^{n-1}}{(\epsilon^{n-1} A + 1)} \xi \qquad \text{A-29}$$

The dimensionless "temperature jump" at the end-walls - i.e. the amount by which T_w^4 at $z = 0$ differs from T_h^4, expressed as a fraction of the total fourth power temperature difference, is equal to $(2(\epsilon^{n-1} A + 1))^{-1}$. It is clearly small for A large, although in the specular case (n=2), it approaches 1/2 as $\epsilon \to 0$, regardless of A. The heat transfer corresponding to this temperature distribution is readily shown from A-15 to be given by:

$$h_T = \frac{1}{\epsilon^{n-1} A + 1} \frac{\sigma(T_h^4 - T_c^4)}{(T_h - T_c)} \qquad \text{A-30}$$

Using the result of Hollands this can be extended to cases where ϵ_h and ϵ_c are not unity, as discussed in Section 3.

A-6 Analytic Solution Using Temperature Linearization

The temperature linearization assumption is given by equation 3.2:

$$T_w^4 \approx T_c^4 + \frac{(T_h^4 - T_c^4)}{(T_h - T_c)} (T_w - T_c) \qquad \text{A-31}$$

By substituting this equation for T_w^4 into the governing equations for the 1D case, using the exponential kernel approximation and non-dimensionalizing according to:

$$\varphi = \frac{T_w - T_c}{T_h - T_c} \qquad \text{A-32}$$

$$\beta_i = \frac{J_i}{\sigma(T_h^4 - T_c^4)} \qquad i = w,c, \text{ and } h. \qquad \text{A-33}$$

and

$$Y_i = \frac{\sigma T_i^4}{\sigma(T_h^4 - T_c^4)} \qquad i = h \text{ and } c \qquad \text{A-34}$$

one obtains the governing equations

$$\beta_w = \epsilon Y_c + \epsilon \varphi + (1 - \epsilon) \delta_{2n} \left\{ \beta_h \frac{e}{2}^{-b\xi} + \beta_c \frac{e}{2}^{-b(A - \xi)} + \int_o^A \beta_w e^{-b|\xi - \eta|} d\eta \right\} \qquad \text{A-35}$$

$$\beta_h = \epsilon_h Y_h + (1 - \epsilon_h) \left\{ \beta_c e^{-bA} + \rho_h \int_o^A \beta_w(\eta) 2e^{-b\eta} d\eta \right\} \delta_{2n} \qquad \text{A-36}$$

$$\beta_c = \epsilon_c Y_c + (1 - \epsilon_c) \left\{ \beta_h e^{-bA} + \rho_c \int_o^A \beta_w(\eta) 2e^{-b\eta} d\eta \right\} \delta_{2n} \qquad \text{A-37}$$

$$\frac{1}{W} \frac{d^2\varphi}{d\xi^2} = (\varphi + Y_c) + \beta_h \frac{e}{2}^{-b\xi} + \beta_c \frac{e}{2}^{-b(A - \xi)} +$$

$$\int_0^A \beta_w(\eta)\, e^{-b|\xi - \eta|}\, d\eta \qquad \text{A-38}$$

where W is defined by 3-5. Differentiating A-38 twice and combining the result with the original A-38 and A-35 there results

$$\frac{d^4 \varphi}{d\xi^4} - P \frac{d^2\varphi}{d\xi^2} = 0 \qquad \text{A-39}$$

with P being given by equation 3-4. A-39 has general solution:

$$\varphi = \gamma_1 + \gamma_2 \xi + \gamma_3 e^{P\xi} + \gamma_4 e^{-P\xi} \qquad \text{A-40}$$

Evaluation of the constants γ_1, γ_2, γ_3 and γ_4 is achieved by making use of the boundary conditions A-9 and A-10 (which become $\varphi = 0, 1$ at $\xi = 0, A$ respectively) and by substituting A-40 back into equation A-38 to eliminate new solutions introduced by the differentiation procedure. The result of the last step is an equation containing zero on the right hand side and on the left hand side, the sum of two independent exponentials in ξ, each having coefficients which are expressions containing the set γ_i. In order for this equation to be identically true, the two coefficient expressions must be identically equal to zero. This gives two additional equations for the four γ_i so that they can in principal be solved. However, these equations contain the radiosities β_h and β_c which are still unknowns and hence a full solution is not yet realized, two more equations being required. This last pair is obtained by substituting A-40 into A-36 and A-37. If one now treats β_h as γ_5 and β_c as γ_6, there results finally six linear equations in the six unknown γ_i's whose solution can now be obtained. The coefficients of these six linear equations are given in Tables 3-1 and 3-2. Equation A-40 then substituted into A-15 gives

the equation for the heat transfer - namely equation 3-3.

A-7 Finite Difference Solution

To obtain results from the "Numerical Theory", the differential rings along the side-wall in Figure A-2 were replaced by discrete rings of extent Δw. In addition, the top and bottom plates were divided into several annular elements. The equations described in the previous sections are, for simplicity, written for the special case of a single element representing the top and bottom respectively; the description in this section will be for this special case also, but the generalization is straightforward. Over each discrete area, the radiosity was assumed constant. The integrations over the range $0 \leq z' \leq L$ in equations A-1 to A-3 were thus replaced by a summation of integrals over the individual elements. The assumption that the radiosities were uniform over each element permitted each of the integrations to be carried out analytically using the angle factors presented in Section A-2.

It is convenient to describe the numerical solution method first for the 1D approximation (Section A-3) and later indicate the generalizations required to include the two-dimensional effects. For the 1D case an initial side-wall radiosity distribution J_w was assumed to start the solution. Equations A-2 and A-3 are combined and rewritten in forms which relate J_c and J_n respectively to the specified temperatures T_h and T_c and to J_w; these equations were solved for values of J_h and J_c using the "guessed" J_w distribution. The conduction-radiation balance at the wall, given by equation A-20 becomes (for ϵ not identically unity),

$$\frac{k_e (A_g + A_s)}{2\pi R} \frac{d^2 T_w}{dz^2} = \frac{\epsilon}{(1 - \epsilon)} \{\sigma T_w^4 - J_w(z)\} \qquad \text{A-41}$$

The solution to this equation, which yields T_w, requires iteration because of the appearance of T_w^4 on the right-hand side. With new values of J_h, J_c and T_w now available, equation A-1 was solved for the new distribution of J_w. This completes one iteration cycle. With the new J_w distribution as the starting point, the cycle was repeated until convergence was achieved.

Allowing for two-dimensional conduction in the analysis requires that the gas inside the cylinder in Figure A-1 be divided into elemental volumes, with one temperature unknown allocated to the nodal point located at the centre of each volume. Non-uniform volumes were used to permit a better resolution of the temperature in the gas near the solid side-walls and end-walls. Performing an energy balance for each volume results in the set of algebraic equations which constitute the finite-difference analog to equation A-6 . Equations A-8 to A-10 provide three of the required four boundary conditions. The fourth is provided by the requirement of temperature and heat flux continuity at the solid surface. Making the approximation that the temperature across the side-wall is uniform at $T_w(z)$, this constraint is expressed by the finite-difference analog to the equation

$$\frac{k_w A_s}{2\pi R} \frac{d^2 T_w}{dz} = \frac{\epsilon}{(1 - \epsilon)} (J_w - \sigma T_w^4) - k_g \left(\frac{\partial T}{\partial r} \right)_{r=R} \qquad \text{A-42}$$

where $T_g = T_w$ at $r = R$.

The 2D problem was solved in the same sequence as before except that, rather than finding T_w from equation A-41, it was found from the solution of the heat conduction equation just described.

Extensive convergence and grid-independence studies were carried

as described in [18]. Based on these, calculated heat transfer rates were considered to be accurate to about 1%.

The finite difference approach has the disadvantage that, like experiments, numbers are obtained as solutions rather than analytical expressions. On the other hand it has the advantage of supplying essentially exact answers to the model described by the set of governing equations, and can be used to provide insight into the validity of the various approximations that are required to obtain analytical solutions. Based on comparisons between the numerical and analytical theories, it was concluded that the 1D approximation was remarkably accurate, that the separable kernel approximation was excellent for the diffuse side-wall case, but less accurate for specular side-walls, and that the end-wall radiosities J_h and J_c were indeed very nearly uniform.

☆ U.S. GOVERNMENT PRINTING OFFICE: 1979—640-189/ 1323